“Smartphone Enabled Biomarker Sensing and On-Demand Drug Delivery using 3D Printed Hollow Microneedle Arrays”

by

Joel Alexander Ninan

B.S. Aerospace Engineering, University of Arizona, 2019

A Project Report Submitted in Partial Fulfillment of the Requirements for the Degree of

Master of Engineering

in Mechanical Engineering

Supervisory Committee

"Smartphone Enabled Biomarker Sensing and On-Demand Drug Delivery using 3D Printed Hollow Microneedle Arrays"

by

Joel Alexander Ninan

B.S. Aerospace Engineering, University of Arizona, 2019

Supervisory Committee:

Dr. Mohsen Akbari, Department of Mechanical Engineering, University of Victoria

Supervisor

Dr. Somayeh Fardindoost, Department of Mechanical Engineering, University of Victoria

Committee Member

Table of Contents

LIST OF TABLES

LIST OF FIGURES

ABSTRACT

Remote health monitoring and disease treatment are pivotal in advancing health equity, reducing geographical and socioeconomic barriers, and providing universal access to quality care. By enabling continuous, personalized healthcare, this paradigm addresses disparities, offering timely interventions for individuals in underserved or remote locations. Microneedle arrays (MNAs) stand at the forefront of this revolution, enabling painless, minimally invasive access to interstitial fluid for both diagnostics and drug delivery.

This paper presents a groundbreaking theranostic wearable system, leveraging digital light processing (DLP) 3D-printed hollow microneedle arrays fabricated using PEGDA hydrogel, equipped with colorimetric sensors for the quantitative analysis of key biomarkers, including pH, glucose, and lactate, directly from the skin's interstitial fluid. The system incorporates a remotely activated, smartphone enabled, ultrasonic atomizer-driven mechanism for on-demand drug delivery, enhancing portability by eliminating the need for complex mechanical pumps. This integrated approach simplifies point-of-care treatments and expands the possibilities for remote patient management.

The accompanying smartphone application seamlessly interfaces with the system, enabling real-time monitoring and drug administration. Demonstrated results include precise detection of pH (3–8 mM), glucose (up to 16 mM), and lactate (up to 1.6 mM), as well as enabling the effective administration of drugs in response to biomarker fluctuations. The system's drug delivery performance was validated using on-demand on/off tests and its biocompatibility using a scratch assay, highlighting its potential for treating chronic diseases requiring sustained therapy.

This innovative platform not only addresses key challenges in drug delivery but also opens new pathways for non-invasive health monitoring, offering a transformative solution for the long-term management of chronic conditions.

ACKNOWLEDGEMENTS

I would like to express my sincerest gratitude to Dr. Mohsen Akbari, for giving me an opportunity to enroll in graduate studies at the University of Victoria and perform research in a lab facility.

I would like to thank my mother and father, who have supported me through thick and thin, and my sister who re-taught me the importance of hard work.

I am profoundly grateful towards Dr. Mahmood Razzaghi, who I got to work with and guided me through this project and beyond, and for his and Dr. Akbari's conceptualization and early work in the project. I also wish to express my warmest gratitude towards Dr. Mostafa Azimzadeh and Esfandyar Askari, for collaborating on the project, specifically on mechanical strength testing and biocompatibility tests such as scratch assay and cell viability assay, which are crucial parts that make up the entire project. I would also like to express my gratitude towards Dr. Meitham Amereh, who taught me how to properly use a pipette and other researchers at LiME who taught me invaluable skills. Lastly, I would like to express my heartfelt gratitude to my dear friends for their wonderful companionship.

NOMENCLATURE

2PP: Two-Photon polymerization

3D: Three dimensional

ABTS: 2,2′-Azino-bis (3-ethylbenzthiazoline-6-sulfonic acid)

CAD: Computer-aided design

DLP: Digital light processing

DMD: Digital micromirror device

FBS: Fetal bovine serum

FDM: Fused deposition modeling

GOD: Glucose oxidase

HRP: Horseradish peroxidase

ID: Implantable device

ISF: Interstitial fluid

LOD: Lactate oxidase

MA: Microneedle

MNA: Microneedle array

MNP: Microneedle patch

MNP: Microneedle patch

OPD: O-phenylenediamine

PB: Presto blue

PEGDA: Poly (ethylene glycol) diacrylate

RGB: Red, green, blue

SC: Stratum corneum

SD: Standard deviation

SEM: Scanning electron microscopy

SLA: Stereolithography

TP: Test paper

WD: Wearable device

WID: Wearable and implantable device

INTRODUCTION

Most people do not like being stuck by a needle, whether for a blood test, vaccination, or blood donation. Yet, judging only by schedules for routine vaccination tests, the average healthy person can expect at least 165 needle sticks over a lifetime [1]. This number increases dramatically for people with chronic illnesses such as diabetes or HIV, where frequent injections are required. While for some, needles are a minor annoyance, for others, it presents a significant challenge, particularly due to trypanophobia—an extreme fear or aversion to blood or needles. It is estimated that this fear affects up to 25% of adults in the US, potentially leading to 16% of the population skipping vaccinations [1]. The Canadian Psychological Association states about 4.5% of Canadians suffer from needle phobia [2]. But people who strongly fear needle sticks tend to avoid doctors and medical care; so, it is likely that the magnitude of this problem is grossly underestimated. This phobia can affect anyone, and the cause is often unknown with some research indicating a cause being- traumatic experience with needles during childhood illness [1]. However, researchers have also found that there may be a genetic component and that trypanophobia sometimes runs in families. This phobia can have serious implications on the health, quality of life and longevity of the population. It affects health, as skipping recommended tests and treatment by avoiding needles can lead to missed diagnoses, poorly monitored medical conditions and undertreatment. It affects quality of life, as anxiety leading to a doctor's appointment or prior to needle injection can deteriorate one's mental health. It affects longevity of one's health, as early detection of cancers, or other chronic illnesses can be unnoticed [1].

The reason why hypodermic needles are used extensively in healthcare is because most biotherapeutic drugs such as peptides, proteins, hormones and natural agents fail to be administered orally due to first-pass metabolism [3]. Some drugs can also harm the liver if ingested orally or they could cause vomiting [4]. Therefore, hypodermic needle injection is used despite pain associated with the insertion of needle. They are used for rapid drug delivery, as drugs are directly absorbed into the bloodstream.

Now, health disparities persist globally due to various factors such as geographic location, socioeconomic status, and unequal access to healthcare. Remote health monitoring and treatment present a promising avenue to address these challenges by bridging gaps in healthcare access [5]. By utilizing technologies like telemedicine and wearable devices, individuals in under-served or remote areas can receive continuous healthcare support, monitor chronic conditions, and access expert consultations from afar [6]. This approach not only improves early detection of health issues but also ensures timely interventions, thereby reducing disparities by offering quality care regardless of geographical constraints or socioeconomic barriers. Additionally, remote monitoring allows healthcare providers to track population health trends, enabling targeted interventions and tailored healthcare strategies to address specific disparities more effectively [7].

Recent progress in skin-interfaced wearables with real-time detection and drug delivery capabilities facilitates ongoing biochemical monitoring and personalized healthcare. Many skin-

interfaced wearable devices have been developed for real-time biomarker detection and health monitoring [8] [9] [10] and health monitoring integrated with drug delivery [11] [12] [13].

Microneedle-based sensors offer an alternative to conventional blood-based techniques by focusing on interstitial fluid (ISF) in the skin, which shares a similar biomarker profile with blood [14]. Devices utilizing test paper-microneedle patches (TP-MNP) have been developed to perform RGB analysis of metabolites in ISF [15], and wearable devices with electronic sensors have been demonstrated for wireless and continuous real-time sensing of metabolites in ISF, showcasing significant potential in non-invasive health monitoring [16].

Microneedle arrays (MNAs) or microneedle patches (MNPs) are medical devices with micron-scaled needles that have been developed to administer vaccines, drugs, and other therapeutic agents [17]. Unlike traditional hypodermic needles, microneedles are minimally invasiveness, offers near painless penetration, induces mild inflammation, and ensure prolonged treatment effectiveness, making them ideal for drug delivery without the need for a skilled professional [18]. MNAs have also shown significant potential for collecting ISF for diagnostic purposes [19].

Various types of MNAs—solid, coated, hollow, dissolving, and hydrogel-forming—have been successfully developed in recent years [20]. Solid MNAs are popular and prevalent in collagen induction therapy [21] and coated MNAs, limited to <1mg doses [3], face constraints for on-demand drug delivery. Dissolving MNAs are made of biodegradable polymers and encapsulate drugs for release after degradation, while hydrogel-forming MNAs are mainly used for diagnostic applications [22] [23]. Hollow MNAs are particularly suitable for on-demand drug delivery due to their design mimicking hypodermic needles and their ability to handle larger drug volumes and faster delivery rates, making them ideal for drug delivery systems already proven effective for proteins, vaccines, and other higher-weight compounds [24] [25] [26] [27].

Conventional manufacturing techniques for MNAs are micro-milling utilizing wet and/or dry etching [16] [28], photolithography [29], molding based approaches [30], cleanroom free molding [31], injection molding [32], laser patterning [33], lithography [34], photolithography incorporating elastic-capillary-driven self-assembly mechanism [35], etc. However, such manufacturing techniques for MNAs are often labor-intensive and involve multiple steps, limiting cost-effectiveness. 3D printing, a relatively recent approach, offers many advantages such as precision, resolution, and the ability to fabricate intricate structures [16] [36]. This makes it a suitable method for producing diverse MNAs for both diagnostic and drug delivery applications. Thus, techniques like digital light processing (DLP), stereolithography (SLA), and fused deposition modeling (FDM) have been successfully employed in the manufacturing of MNAs for both drug delivery and also for detection and diagnostics [37] [38] [39] [40] [41].

In this project, a wearable theranostic device was developed that utilizes hollow MNAs for biosensing and on-demand drug delivery facilitated with the help of a smartphone application. The system utilizes hollow microneedles in the form of a MNA fabricated using DLP 3D printing, integrated with an ultrasonic atomizer membrane for on-demand medication administration. The patch-based system will enable transdermal drug delivery, offering an alternative to traditional hypodermic injections. For biosensing, the wearable device utilizes another hollow MNA. Its

capability was rigorously assessed through comprehensive pH, glucose and lactate measurements. This evaluation highlights the accuracy and efficacy of the MNA system in capturing a few key biomarkers that are crucial for health monitoring and disease management. Furthermore, to investigate the practicality of on-demand drug delivery, a critical aspect of the MNA wearable device, through a series of experiments, we successfully demonstrated the system's ability to deliver both small fluorescent molecules as well as larger biomolecules in a scratch assay. This showcases the versatility and effectiveness of a mechanical pumpless wearable MNA in administering a spectrum of therapeutic agents, from conventional pharmaceuticals to more complex biomolecular compounds, with precision and control. This work represents a significant step forward in wearable biomedical technology, offering a promising platform for real-time biosensing and tailored drug delivery. The integration of biosensing and drug administration functionalities in a single wearable device holds immense potential for advancing personalized healthcare and revolutionizing treatment modalities for various medical conditions.

Intellectual merit of the project

Although there has been a fair amount of research done that study the design, development and use of microneedles over the last two decades which has led to the development of various single use patches for drug delivery, little work has been done that explores on-demand drug delivery. Moreover, even less work has been done that explores on-demand drug delivery that can be activated remotely, such as with a smartphone application. A sizeable fraction of the world population suffers from chronic illnesses such as diabetes, high-blood pressure, high-cholesterol, cancer, mood and/or anxiety disorders with estimates stating that over 95% have one or more ailments and one third have more than five ailments [42]. Drugs used to treat such diseases must be administered routinely. Also, patients are hospitalized for various health reasons such as post accidents, and pre- and post-surgery, which also require frequent drug administration. This device offers detection of critical health biomarkers and allows painless and on-demand drug delivery for a patient. Thus, much of the negative aspects of hypodermic needles such as fear and anxiety and disposal of biohazardous waste that require careful disposal is reduced. This device has the potential to be further improved into a fully functional and easy to use self-administrable device comparable to a home use blood pressure monitor or a glucose meter. Although PEGDA has been used extensively in microfluidics research, little work has been done in using it for microneedle fabrication. Even less work has been published for producing hollow microneedles, which are essential for the on-demand high drug load capability of this device. The research performed sheds light on optimized geometry, such as lumen size, and fabrication methods to make such microneedles. The device also uses a piezoelectric ultrasonic membrane based micropump, which hasn't been used previously with microneedles for transdermal drug delivery. Moreover, it also uses an easy-to-use smartphone assisted colorimetric sensing method to detect concentrations of some key biomarkers in ISF. Biomarker sensing is performed with the smartphone app and with single use low-cost reagent coated paper strips onto the device. The color change that denotes biomarker concentration can be observed visually and can be read out compared to a reference sheet, much like pH strips. Furthermore, the smartphone app reads out the biomarker concentration at varying lighting conditions as it normalizes the average colour of the test strips. Thus, the simplicity of this device offers potential in serving underserved or low-income regions as it is low-cost and easy-to-use.

Broader Impact on Canadians and Human Health

Sixty-five percent of adults in Canada, aged 19 and over, have at least one chronic condition with the most common in both males and female being dyslipidemia, followed by depression, obesity and hypertension [43]. In 2021-2022, there were almost 2.9 million acute inpatient hospitalizations in Canada with the average length of stay being 7.2 days [44]. Needle phobia is observed in a sizable fraction of Canadian and world population which prevents some from getting vaccinations, injections and blood work. A painless, simple, easy to use device, which can serve as an alternative to injections can solve most of these issues. This can lead to better overall well-being of people. Additionally, the development of such a device is an added tool to the world of drug-delivery methods which could one day be a common sight in hospitals and at homes. Work done that lead to the development of this device can potentially help in the development of other technologies that can benefit human health and well-being in the future.

There are various reasons that indicate why such a product will benefit Canadian society. A major reason why single use transdermal patches are popular is the ease of application. They provide a slow and controlled release of medication to the patient. However, only medication whose molecules are small enough to penetrate the skin can be delivered through this method as the stratus corneum is an effective barrier. Microneedle transdermal patches, that consists of an array of microneedles allows a more versatile range of molecules and compounds to be passed and absorbed through the skin. These patches also allow a controlled release of medication and can be applied without the assistance of a medical professional. Solid, coated and hydrogel-forming microneedles are all proven designs that effectively deliver drugs through the skin. But they are limited by the amount of medicine that can be loaded, and they cannot be reused or be used for an on-demand drug delivery device. The device designed by S A. Burton et. al. at 3M's Drug Delivery Systems Division was the only product that reached pre-clinical trials and failed to become commercially manufactured. There are numerous reasons one can state why this might have happened. This includes an inefficient design and a lack of funding or interest by the company to commercialize such a product. The active/powered pumping proposed in this device could address issues faced by the development of the product by 3M. It allows fine control over the flow rate as ultrasonic membrane pumps are known for their ability to offer precise output and feedback control by varying potential and current flow. It also could push air, so little drug could be left within the microchannels. Additionally, its sensing capabilities enable monitoring of biomarkers and are proposed as an alternative to other bulkier detection methods. As it is statically known that a large fraction of Canadian and North American population has needle phobia, such a device could benefit both physical and mental health of the general population. Individuals that must undergo frequent injections that have a fear of needles could experience a relief with such a device as they do not have to dread their routine. Moreover, the use of such a device among younger populations, particularly kids, could prevent the formation of needle phobia in adulthood as it eliminates childhood trauma related to needles to some extent. There are also environmental benefits to the development and such of such a device that cannot be ignored, which could affect not just Canadian, but the globe. WHO reported that 16 billion injections are administered each year globally [45]. The global syringe market is valued at USD 16.9 billion in 2023 and is expected to grow to USD 25.63 billion [46]. As these are one-time-use products, the plastic pollution footprint of this industry is huge, not to mention the difficulties of proper disposal of hypodermic needles and syringes. Such a type of "reusable" and on-demand drug delivery product can help mitigate this issue to an extent, given its scope of application.

BACKGROUND LITERATURE AND SIGNIFICANCE

Skin

Skin is the largest organ in our body, and it accounts for roughly 15% of the total body mass [47]. It acts as a highly impermeable region of the human body and is considered as critical protective barrier from the external environment and plays an important homeostatic role [47].

The skin has three main layers: the epidermis, dermis and hypodermis. The epidermis is the thinnest layer of the skin, but it is responsible for protecting us from the outside world [48]. The outermost layer of the skin, the stratum corneum (10-20 μm), which is part of the epidermis, is made up of dead cells, which play a vital role in deterring the entry of macromolecules [3]. The epidermis varies in thickness and can be as thick as 1.5 mm (sole of the foot) [48] or as thin as 0.07 mm eyelids and genitalia [49]. The epidermis contains viable cells without extensive nerve networks [3], hence needles inserted to this point should cause minimal pain. The dermis is a tough but elastic support structure that houses nerves, blood vessels, lymphatics, and cutaneous appendages (pilosebaceous units, eccrine and apocrine sweat glands) [49]. It is thicker than the epidermis and it varies in thickness averaging 1-4mm [49]. The hypodermis (Subcutaneous Tissue) is the innermost layer of skin. It has many functions such as connecting dermis to muscles and bones, insulation, shock absorption, and storing energy in fat cells (adipocytes) [50].

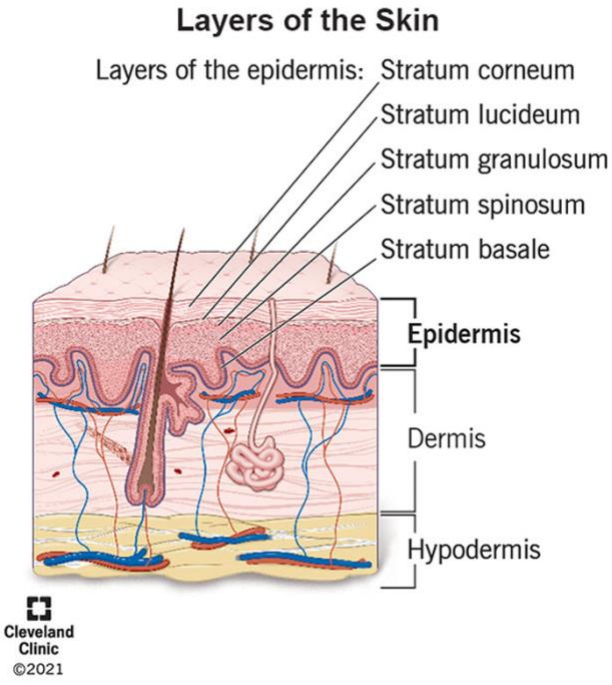

Figure 1: Layers of the Skin [48].

In recent times, the skin has been recognized as an organ that aids in the delivery of a wide range of drug molecules into the skin through intradermal drug delivery and across the skin into the systemic circulation in the form of transdermal drug delivery [47]. The skin's position and large surface make it a suitable and non-invasive location not only for supplying therapeutic agents but also for sampling interstitial fluid for biomarker detection [24]. Using the skin as the drug administration site is an attractive option for distributing therapeutics such as vaccines, drugs, biomolecules, and difficult-to-deliver small molecules [24]. A fluid drug delivered to the epidermis can travel to the dermis through passive diffusion as skin interstitial fluid connects the epidermis and the dermis [51].

Microneedles

In recent times, the use of "microneedles" for transdermal drug delivery for point of care diagnosis, prognosis and treatment is seen as an area of great research interest. Although microneedle technology was originally conceptualised and patented in the 1950s, it took some time for the benefits of microneedles to be widely recognised [24]. It was not until 1998 that a report was released that looked at the potential use of microneedles for vaccines [24]. Since then, the number of investigational studies on MNs has grown considerably. There has been considerable progress in recent decades, including advances in strategies of microneedle fabrication and the assessment of MNs in clinical applications to satisfy the complex requirements in actual use [24]. Essentially, MN-based delivery and sampling are pain-free, non-invasive, and self-administered techniques that serve as an alternative to hypodermic needles, providing enhanced patient compliance [26]. Figure 2 shows the insertion depth of a microneedle patch on skin.

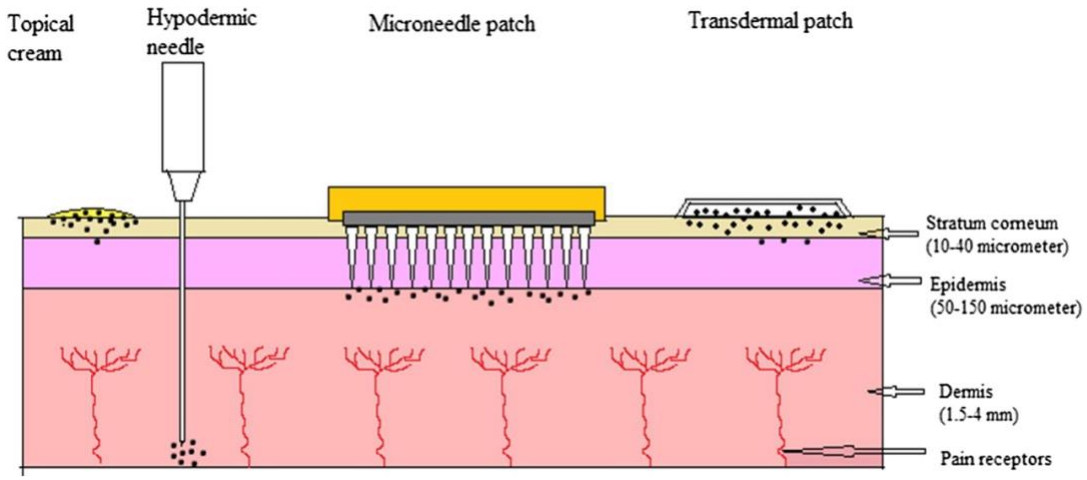

Figure 2: Microneedle patch insertion depth on skin compared to hypodermic needles and transdermal patches [26].

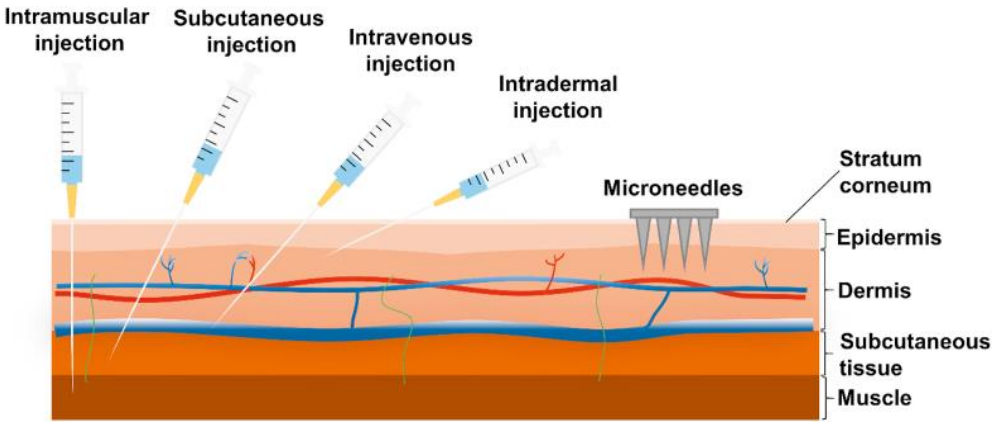

Figure 3: Schematic illustration of protein and peptide drug delivery by conventional injections and microneedles [52].

Microneedles or microneedle patches are micron-scaled medical devices used to administer vaccines, drugs, and other therapeutic agents [17]. They are constructed through various methods, usually involving photolithographic processes or micro-molding [25]. Typically, microneedles are applied through small arrays that encompass a collection of microneedles, ranging from only a few microneedles to several hundreds, which are attached to an applicator [53]. Research has shown that there is a limit on the type of drugs that can be delivered through the skin. Only compounds with relatively low molecular weights can penetrate the skin and compounds that weigh more than 500 Da (atomic mass) cannot penetrate the skin [54]. However, many common drugs that are administered to chronic patients have relatively low atomic masses. Hence, the use of this technology is feasible for this device.

Types of Microneedles

Since their conceptualization, various kinds of microneedles have been developed, each with its own set of advantages and disadvantages. They can be classified as solid, coated, hollow, dissolving, and lastly, hydrogel forming [52]. Each type of MNs has been extensively studied for transdermal drug delivery and continues to be an ongoing filed of research.

Solid Microneedles

Solid MNs usually need a two-step operation for drug delivery. Briefly, solid MNs are first inserted into the skin and subsequently removed to form temporary microchannels. Then, a suitable pharmaceutical dosage form, such as gel, cream, or ointment is applied to the previously formed microchannels [25] [52] [55]. Solid MNs should offer sufficient mechanical strength for successful skin pretreatment by selecting the materials of MNs [25]. Typically, solid MNs are fabricated from silicon and metal [56] [57]. But, although silicon and metal have good properties for solid MNs fabrication, but they may be unsuitable for transdermal drug delivery as their non-biodegradable nature may cause safety issues after being inserted into the skin. In contrast, polymeric materials usually have good biocompatibility. Various polymeric materials, such as polylactic acid (PLA),

polymethylmethacrylate, polycarbonate, and carboxymethylcellulose (CMC) have been developed to prepare solid MNs as an alternative to non-biodegradable materials [52].

Solid MNs deliver drugs by passive diffusion through the generated microchannels in the skin. Therefore, the length and density design of solid MNs used for skin pretreatment will affect drug penetration [58]. Moreover, the properties of the drugs also affect delivery efficiency. Contrary to the traditional transdermal delivery, the microchannels formed by the pretreatment of solid MNs will increase the penetration of hydrophilic compounds [59]. The molecular weight of drugs can also affect passive transport by using solid MNs. For example, it was observed that the transport rate of a larger molecular weight (72 kDa) compound was much lower than the compounds with molecular weight of 10 kDa and 538 Da [60].

Solid MNs have some inherent drawbacks. A two-step administration process including pretreatment with MNs array and then application of pharmaceutical preparations is considered inconvenient, and it may cause imprecise dosage. Due to the negative impact on patient compliance, drug delivery strategies based on other MNs have now become more prevalent [52].

Coated Microneedles

To avoid a two-step application process, solid MNs are coated with drugs on the surface of the needles to obtain coated MNs. Coated MNs provide a more convenient and controllable way for transdermal drug delivery. When coated MNs are inserted, the drug coating layer will dissolve and further deposit the active pharmaceutical ingredients into the skin, then the MNs can be removed [26].

Coated MNs are typically prepared using metal or silicon; but to avoid the use of less biocompatible materials, polymeric coated MNs have also been widely investigated. For example, coated solid microstructure transdermal system (sMTS) were developed for Peptide A delivery where 250 μg of Peptide A was coated on a patch containing 316 needles [61]. Successful transdermal delivery was achieved with demonstrated bioavailability being similar to subcutaneous injection [61].

Several techniques, such as spray coating, dip coating, and piezoelectric inkjet printing, have been demonstrated for the coating of MNs [62]. Spray coating and dip coating are the most common methods using an aqueous drug solution with high viscosity to retain more drugs on MNs surface. The main challenge is how to ensure sufficient therapeutic agents are uniformly coated. Therefore, it is important to optimize the coating process and formulation composition. Surfactants, viscosity enhancers, and peptide stabilizers are usually required in the formulations, to ensure coating stability and uniformity of the drug. Since most biomolecules are hydrophilic, the coating solution is usually aqueous [52].

Although the mechanical strength of coated MNs is usually retained, their tip sharpness is reduced with the drug loading, which may influence the skin penetration ability [63]. Moreover, coated MNAs are limited to $\leq$1 mg doses and face constraints for on-demand drug delivery [20].

Hollow Microneedles

Hollow MNs are sub-millimeter devices that act like micron-scale syringes which can penetrate the stratum corneum to allow the flow of liquid formulation into the skin [20]. In the simplest form, drug delivery using hollow MNs is achieved through passive diffusion. Since the passive diffusion rate in dense tissues is relatively low, faster transport rate through pressure-driven flow or diffusion has been successfully achieved [64] [65]. Consequently, compared with solid MNs, hollow MNs can allow the administration of larger doses, and simultaneously provide an exact transport rate [20] [66]. They offer control over drug flow rate as release pressure can be controlled, and they can also deliver higher molecular weight compounds such as proteins, vaccines and oligonucleotides [26].

Hollow MNs usually need a more complicated fabrication technology. In addition to preparing a needle with suitable inner holes, hollow MNs should also be combined with some form of drug reservoir. Such a system can use a passive or active pumping system to trigger drug release.

Shown below is an image of a hollow MNA produced with a combination of UV photolithography and replica molding methods.

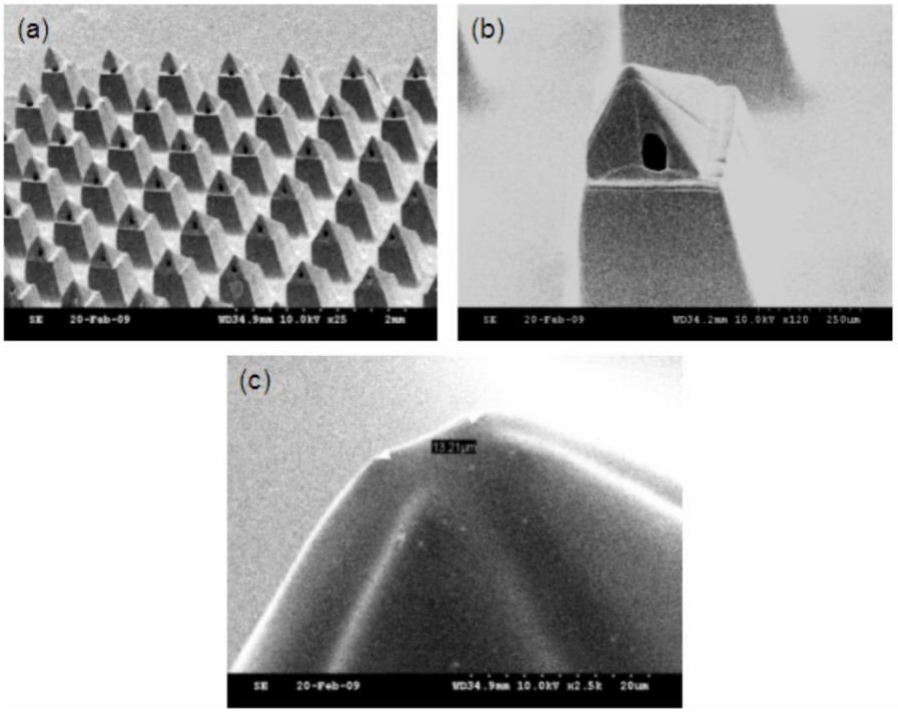

Figure 4:A SEM image of bird-eye's view of fabricated microneedle array coated by 15 nm Cr/150 nm Au for SEM imaging. (b) A SEM image revealing the pyramidal tip with a lumen opening and upper shaft. (c) A high magnification (2.5K×) SEM image of the tip of the pyramid. The tip diameter for this microneedle is 13.2 µm, while the tip diameter generally ranges from 15 to 25 µm across the array [51].

Shown below is a figure that demonstrates the working of the types of microneedles.

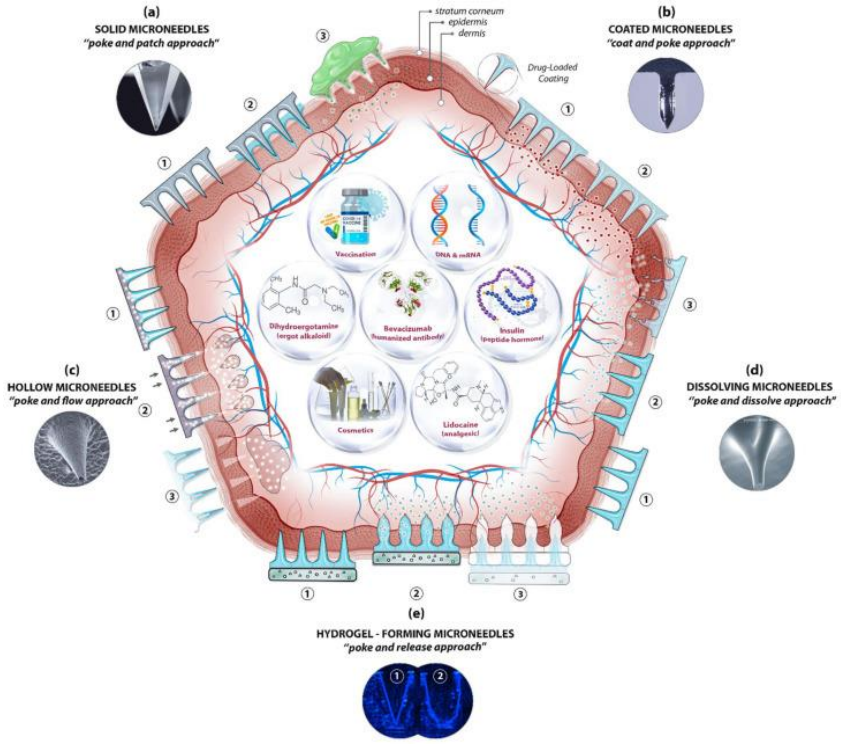

Figure 5: A schematic diagram of microneedle (MN)-based drug delivery approaches with the cross section of the upper layer of the skin. The approaches are (a) solid MNs, (b) coated MNs, (c) hollow MNs, (d) dissolving MNs, and (e) hydrogel-forming MNs [24].

3D Printing of Microneedles

The advent of 3D printing has revolutionized the field of microneedle fabrication, offering a versatile and cost-effective alternative to traditional manufacturing methods. Unlike conventional techniques—such as photolithography, micro-milling, and injection molding—which are often time-consuming, labor-intensive, and expensive, 3D printing provides precise control over the geometry and structural features of microneedles. This technology allows for rapid prototyping and customization, enabling researchers and manufacturers to optimize microneedle design for various biomedical applications- including drug delivery, diagnostics, and biosensing.

3D printing techniques, such as stereolithography (SLA), digital light processing (DLP), and fused deposition modeling (FDM), and two-photon polymerization (2-PP) have been particularly effective in creating microneedle arrays with intricate and reproducible structures. These methods ensure high-resolution fabrication, essential for the micrometer-scale features required for safe and effective skin penetration. The growing accessibility of 3D printers and advancements in

biocompatible printing materials have further expanded the potential for personalized healthcare solutions and large-scale manufacturing.

Fabrication Techniques for 3D Printed Microneedles

The utilization of three-dimensional (3D) printing represents a relatively recent approach for creating MNAs, as it offers various advantages compared to traditional methods. Advances in printing resolution, precision of features, and the accessibility of cost-effective printing materials has enabled the production of diverse types of MNAs using 3D printing [67] [36] [68] [69]. This technology allows for the fabrication of intricate structures with precise control over geometry, form and size, as well as mechanical and biological properties [70] [71] [72]. Various 3D printing techniques, such as high-precision stereolithography (SLA), digital light processing (DLP), fused deposition modeling (FDM) and Two-Photon Polymerization (2PP) have been employed to manufacture MNAs [37] [38] [39] [73].

Stereolithography

Stereolithography is a 3D printing technology that produces parts in a layer-by-layer fashion using photochemical processes, by which ultraviolet (UV) light causes chemical monomers and oligomers to cross-link together to form polymers [74]. Solid objects of a curable material are printed in thin layers one on top of the other. A programmed movable spot beam of UV light shining on a surface or layer of UV curable liquid is used to form a solid cross-section of the object at the surface of the liquid. The object is then moved, in a programmed manner, away from the liquid surface by the thickness of one layer, and the next cross-section is then formed and adhered to the immediately preceding layer defining the object. This process is continued until the entire object is formed [74]. Typical SLA processes exhibit superior resolution (10-150μm) and surface roughness (0.38-0.61μm) compared to material jetting, material extrusion and powder bed fusion [75].

Digital Light Processing

Digital light processing (DLP®) also uses photocurable resins, to fabricate 3D parts, layer by layer, through spatially controlled solidification by using a projector light (either UV or white light) [76]. In addition, it is possible to tailor the final properties of the printed object by simply changing the photocurable resin formulations [77]. When light is projected onto the resin using DLP technology, instead of being restricted to a spot like the laser-assisting 3D printing, the entire layer is printed immediately, as it uses a projector light. Hence, this technology allows fast printing [78]

[79]. DLP printing technique has a relatively high resolution, which is usually at the micron scale [80]. The resolution of DLP 3D printing partially depends on the material chosen. For example, when the 3D constructs are printed using polyethylene glycol diacrylate (PEGDA MW = 700 da) solely, the XY resolution of the constructs can reach nearly 6 by 6 μm. Meanwhile, the resolution is about 17 μm with bioink containing 10% gelatin-methacrylate (GelMA) and 3×10^6 cells/mL [81].

Fused Deposition Modeling

In this material extrusion process, a continuous filament of thermoplastic or composite material is used to construct 3D parts. The polymer filament is forced through a nozzle where the head is regulated by temperature and heated to the semi-liquid stage and fed over the build plate or previously solidified substance. The product is built layer by layer technique at a constant speed and pressure [82]. Fused deposition modeling is a popular additive manufacturing technology because of its fast production, cost-efficiency, ease of access, broad material adaptation, and capability to produce complex components [82]. Acrylonitrile butadiene styrene (ABS), polylactic acid (PLA), and polycarbonate (PC) are popularly used materials in FDM [82]. Post-processing is a vital process in FDM since the printed parts are not entirely ready for instant usage. After the printing process, the product is taken out from the bed platform, and the supporting structures are removed and undergo post-processing. This process is mainly used to improve the surface quality of the product [83]. In the context of 3D printing microneedles, methods that combines FDM with a post-fabrication etching step to yield ideally sized and shaped needles that are able to insert, break off, and deliver small molecules into skin without the need of a master template or mold have been successfully developed [39].

Two-Photon Polymerization

Two-photon polymerisation (2PP) has been developed in recent years to enable the manufacturing of elaborate structures in the micro and nanoscale. In this specific technology, ultrashort laser pulses from a near-infrared femtosecond laser source are used to selectively polymerise photosensitive resins. The electronic excitation generated by the nearly simultaneous absorption of two photons is similar to that of a single photon with higher energy. This absorption provides a nonlinear energy distribution, centred at the laser's focal point and with negligible absorption outside the immediate area of the laser's focal volume. Upon absorption of this energy, photo-initiator molecules in the resin will begin the polymerisation process at locations known as "polymerisation voxels", where the energy surpasses a certain threshold. In comparison with other techniques, 2PP shows improved geometry control, as well as scalable resolution, reducing equipment, facilities and maintenance costs commonly associated to etching and lithography-based methods. For this reason, researchers have exploited this technique to fabricate solid or

hollow MN arrays using modified ceramics, inorganic-organic hybrid polymers, acrylate-based polymers, polyethylene glycol, and recently, water-soluble materials, with promising results [84].

Applications of 3D Printed Microneedle arrays

SLA printing has been used to create master molds for dissolvable PVP/PVA MNAs for ocular drug delivery [85]. It has been used to make coated MNAs out of a class I biocompatible resin, Dental SG, for intradermal insulin delivery [86] and to make hollow, dissolvable and solid MNAs (made with materials like Dental SG; class IIa biocompatible resin Dental LT clear; and poly(propylene fumarate) (PPF) mixed with diethyl fumarate (DEF)) for transdermal drug delivery [37] [87] [40] [88] [89]. SLA MNAs has been used to make hollow MNAs with e-Shell 200 for transdermal electrochemical sensing [90], to make base substrate for Lab-on-a-microneedle made with VisiJet FTX Green- for rapid detection of biomarkers in finger-prick-blood [91]. It has been used to make hollow MNAs with High Temp resin for blood-free detection of C-Reactive protein and Procalcitonin [92] in ISF. SLA printed microneedles have been used to fabricate hollow MNAs for plant health monitoring using in situ electrochemical analysis by detecting biomarkers like H_2O_2, glucose and pH [93].

DLP printed hollow microneedles made of PEGDA, have been developed for transdermal drug delivery [20] and multiplexed detection of biomarkers, such as pH, Glucose and Lactate in skin ISF [20]. Solid hydrogel MNAs manufactured with DLP have been developed for transdermal drug delivery [94]. Continuous glucose monitoring in ISF with sold MNAs made with biocompatible light sensitive resins has also been successfully demonstrated by in-vivo testing on mice [95]. It has also been used to develop drug delivery systems utilizing hollow MNAs made with biocompatible class I resins (Dental SG), to the buccal tissue as they increase the permeability of actives with molecular weights between 600 and 4000 Da [96].

As FDM printed microneedles have been limited by their resolution and finish, they are less preferred for manufacturing microneedle arrays. However, when combined with a post fabrication chemical etching process, it has been shown that tip sizes as small as 1-55μm can be achieved [39] (Typical resolution without post fabrication steps is 50-200 μm [97]). FDM printed biodegradable MNAs, BPMNAs made with polylactic acid (PLA) with drug absorbed into the polymer matrix (which can also be used as solid or coated MNAs) have been developed to load small molecules for transdermal drug delivery [39]. To facilitate high drug-loading capacity, BPMNAs with a drug reservoir made with PLA have been developed for transdermal drug delivery [98]. Coated PLA MNAs have also been developed for transdermal drug delivery [99].

A major advantage of 2PP is that it can achieve resolutions as low as 100nm [100]. 2PP has been used to mold dissolving and hydrogel forming microneedles with an aqueous blend of PVP and PVA, for controlled drug delivery of model drugs through skin models [84]. It has been used to develop hollow MNAs of organically modified ceramic hybrid materials (Ormocer®) for transdermal drug delivery [101]. 2PP has been used to make hollow MNs with IP-S Photoresist for intracochlear diagnostics [102]. An interesting hybrid method of utilizing 2PP and electrochemical deposition was utilized to fabricate ultra-sharp gold coated copper solid MNA for inner ear drug delivery [103]. It has been used to produce hollow MNAs with Eshell 300, a class 2a biocompatible material popular in the hearing aid industry, for transdermal sensing of electrolytes such as K+ ions [104].

Fabrication Techniques	Materials	Microneedle Types	Advantages	Disadvantages	Applications of 3D Printed MNAs	Minimum Resolution	Cost	Reference
Stereolithography (SLA)	PVP/PVA. Dental SG. Dental LT clear. PPF mixed with DEF. e-Shell 200. VisiJet FTX Green. High Temp resin.	Hydrogel. Coated. Hollow. Dissolvable. Solid.	High resolution.	Relatively expensive. Slow process. Limited materials.	Transdermal drug delivery. Ocular drug delivery. Intrdermal drug delivery. Intarcochlear diagnostics. Transdermal electrochemical sensing. Biomarker detection in blood. Blood free detection of proteins in ISF . Plant health monitoring.	10-150µm.	High.	[37][85][86][87][88][89][90][91][92][93]
Digital Light Processing (DLP)	PEGDA. Biocompatible light sensitive resins. Dental SG.	Hollow. Hydrogel. Solid. Coated.	Fairly high resolution.	Moderate to expensive. Lower resolution and surface finish compared to SLA.	Transdermal drug delivery. Drug delivery through buccal tissue. Multiplexed biomrker detection in ISF. Continuous glucose monitoring.	17µm and above.	Medium.	[20][93][94][95][96]
Fused deposition Modeling (FDM)	PLA.	Solid. Coated. Dissolvable.	Affordable. High throughput.	Low resolution. Often requires post-fabrication processes.	Transdermal drug delivery.	50-200µm. 1-55µm with post-fabrication steps.	Low.	[39][83][97][98][99]
Two-Photon Polymerization (2PP)	PVP/PVA. Ormocer. IP-S Photoresist coated with gold. Eshell 300.	Hollow. Hydrogel. Dissolvable. Solid.	Very high resolution.	Expensive. Slow process.	Transdermal drug delivery. Intracochlear diagnostics. Inner ear drug delivery. Transdermal sensing of electrolytes.	100nm.	Very high.	[84][100][101][102][103][104]

Table 1: Summary of 3D Printing Methods for MNA Fabrication and their Applications.

Challenges and Limitations of 3D Printing Microneedle Arrays

Material selection is pivotal in the performance and safety of 3D-printed microneedles, as it directly influences both biocompatibility and mechanical integrity. Achieving an optimal balance between these factors remains a significant challenge. Biocompatibility is essential, especially in medical applications, where materials must be non-toxic, non-immunogenic, and capable of integrating seamlessly with biological tissues. Common choices include biocompatible resins used in stereolithography (SLA) and biodegradable polymers like polycaprolactone (PCL) for drug delivery applications. However, these materials often face limitations in mechanical strength, which is critical for ensuring microneedles can reliably penetrate the skin without fracturing. The trade-off between mechanical properties and printability poses another challenge. High-resolution

techniques like SLA and two-photon polymerization (2PP) require materials that can be precisely shaped while maintaining sufficient rigidity. Simultaneously, innovations in composite materials, combining polymers with nanoparticles or reinforcing fibers, are emerging to enhance both durability and functional performance. Furthermore, degradation and stability remain key considerations, particularly for dissolvable or biodegradable microneedles. Optimizing materials for predictable degradation profiles while preserving stability during storage is critical for effective drug delivery.

Mechanical strength and durability of 3D-printed microneedles are critical to their effectiveness in applications ranging from transdermal drug delivery to biosensing. Microneedles must withstand the forces involved in skin penetration while maintaining structural integrity. Mechanical failure, such as tip breakage or bending, can result in incomplete drug delivery or compromised sensor accuracy, posing significant risks in clinical settings. This is as weakness of hollow MNAs as they are more fragile than solid MNAs. Achieving the right balance between sharpness and strength is particularly challenging at the microscale. Techniques like stereolithography (SLA) and two-photon polymerization (2PP) enable high-resolution printing but often yield brittle structures due to the inherent properties of photopolymer resins. Researchers are addressing this limitation by developing composite materials and optimizing polymer formulations that offer improved toughness without sacrificing detail.

Durability is also crucial in applications where microneedles are expected to endure repeated insertions or prolonged exposure to biological environments. For instance, microneedles used for continuous monitoring or extended drug release must resist degradation while maintaining functionality. Advances in reinforcing microneedles with nanoparticles or integrating flexible polymers are promising strategies, but challenges remain in consistently achieving both strength and biocompatibility. As a result, the development of mechanically robust yet minimally invasive microneedles continue to be a focus of ongoing research and innovation.

Despite the promising capabilities of 3D-printed microneedles, scaling their production for widespread clinical use remains a significant challenge. High-precision fabrication methods like stereolithography (SLA) and two-photon polymerization (2PP) offer unparalleled resolution but are inherently limited by low throughput and high costs. These techniques require specialized equipment and materials that drive up production expenses, making large-scale manufacturing difficult. For instance, 2PP can produce microneedles with nanoscale precision but is often prohibitively slow and expensive for commercial applications. Scalability also hinges on maintaining consistent quality as production volumes increase. Ensuring uniformity in microneedle dimensions, tip sharpness, and material properties across batches is crucial for both safety and efficacy. Traditional manufacturing processes, like injection molding, offer higher throughput but fall short in delivering the micro-level precision required for advanced designs. This makes it difficult to scale up without compromising performance. Additionally, the economic feasibility of 3D-printed microneedles is affected by material costs, which are often high for biocompatible resins and polymers tailored for microneedle applications. Cost-effective manufacturing solutions may involve hybrid approaches that combine 3D printing with other techniques or innovations that simplify post-processing steps. Overcoming these cost and

scalability barriers is essential for transitioning microneedles from research prototypes to accessible medical devices in broader healthcare markets.

The translation of 3D-printed microneedles from research innovations to approved medical devices faces considerable regulatory and clinical hurdles. Regulatory approval processes for medical devices are stringent, requiring comprehensive data on safety, efficacy, and reliability. For 3D-printed microneedles, this involves demonstrating consistent manufacturing quality, material safety, and predictable performance in clinical settings. The introduction of novel materials or fabrication methods often complicates regulatory pathways, as existing standards may not fully address the unique characteristics of 3D-printed microneedles.

Clinical validation is another critical challenge. Despite promising laboratory results, limited long-term clinical data are available for many 3D-printed microneedles, making it difficult to gain regulatory approval and build confidence among healthcare providers. Large-scale clinical trials are needed to assess both short-term and long-term outcomes, including biocompatibility, patient safety, and device durability. Additionally, the absence of standardized testing protocols for evaluating microneedles' mechanical strength, drug delivery efficiency, and biodegradability further delays regulatory clearance. The path to commercialization also requires navigating the complexities of intellectual property rights, liability concerns, and alignment with global regulatory standards. Addressing these challenges through collaboration between researchers, manufacturers, and regulatory bodies will be key to accelerating the development and market adoption of 3D-printed microneedles.

EXPERIMENTAL SECTION

Materials

To produce the MNAs and the test strips, the following materials were used:

PEGDA (Mw 250 Da) monomer, phenyl-bis-(2,4,6-trimethylbenzoyl)-phosphine oxide (Irgacure 819), Sudan I, bromocresol green dye, o-phenylenediamine (OPD), 2,2′-Azino-bis(3-ethylbenzthiazoline-6-sulfonic acid) (ABTS), horseradish peroxidase (HRP), glucose oxidase from *Aspergillus niger*, lactate oxidase from *Aerococcus viridans*, chitosan, acetic acid, and paraffin wax, were all purchased from Sigma- Aldrich. The filter paper was sourced from GE Healthcare Life Sciences (Whatman TM). Potassium iodide was purchased from Caledon Laboratory Chemicals. Sodium citrate was purchased from Bio Basic Canada Inc, and agarose purchased from FroggaBio. Also, B27 supplement was purchased from Thermo Fisher Scientific.

To facilitate mechatronic drug delivery aspect of the wearable device, the following materials were used:

An Arduino nano microcontroller, L298N motor driver, TB6612FNG motor driver, HC-05 Bluetooth module, HM-10 BLE module, mini-breadboards and wire connectors, were sourced from RobotShop. 20 mm ultrasonic membrane sets were sourced from Amazon.

Both android and iOS smartphones were used to test the application enabled functionally of the device.

Study Design

This study aimed to investigate the possibility of using an integrated device for the sensing of biomarkers in ISF and on-demand drug delivery. In this regard, different assessments were performed on both sensing and drug delivery sets. Based on the outcomes, the integrated device can also be facilitated as a closed-loop sensing and drug delivery device, if needed so.

Fabrication of MNAs

To prepare the PEGDA-based bioink, a 2 wt% solution of Phenyl-bis(2,4,6-trimethylbenzoyl)-phosphine oxide as a photo-initiator and 0.04 wt.% of Sudan I as a photo-absorber was dissolved in PEGDA 250. The 3D models of MNAs were generated using SOLIDWORKS® software, and the models were sliced into cross-sectional images using CHITUBOX software. The 3D printing of both sensing and drug delivery MNAs were performed using a commercial DLP printer (Anycubic Photon Mono 4K). A layer height of 20 µm, was used for the printing process.

Following 3D printing, the MNAs were subjected to a 5-minute ethanol rinse at ambient conditions to wash out and eliminate any unreacted bioink. Subsequently, the MNAs were thoroughly air dried at ambient conditions. Finally, a post-curing step was carried out for 10 minutes using a 405 nm wavelength UV oven to ensure the fixation of their shape.

Fabrication of Test Papers

Filter paper was chosen as the host substrate for sensing reagents comprising chromogenic dyes, HRP, and respective oxidases of biomarkers. The filter paper was cut to have the width equal to each quadrant of the sensing microneedle and approximately thrice the length to aid in insertion and removal into the sensing quadrant. Paraffin wax was coated onto each filter paper, such that a square section was left for sensing. Then, the filter papers were heated to 90 ℃ for 5 minutes to ensure that the wax penetrated deep into the filter paper such that the reagents would remain in the sensing section of the filter paper after being drop-cast.

The sensing reagents for lactate were 10 mM OPD, 0.15 mg/mL of HRP, and 5 mg/mL of lactate oxidase (LOD) in DI water. The sensing reagents for glucose were 100 mg/mL of potassium iodide in sodium citrate buffer (pH 6), 0.3 mg/mL of HRP, and 10 mg/mL of glucose oxidase (GOD) in DI water. For pH, the sensing reagent was 0.04 wt% bromocresol green in DI water. For lactate and glucose, the test papers were first modified with 0.5 µL of chitosan solution (1 mg/mL in 0.2% acetic acid). After drying, 0.5 µL of chromogenic dye solution, HRP, and the respective oxidases were uniformly drop-cast onto the test papers with a pipette; followed by the addition of 0.5 µL of chromogenic dye solution. To prepare the pH sensing quadrant, 1 µL of chromogenic dye solution was drop-cast onto the test paper. After drying, to avoid dye oxidation or enzyme degradation, the papers were stored in sealed hermetic bags at 4 °C. These methods were based on work published by D.D. Zhu et. al. (2022), in their paper titled “Colorimetric microneedle patches for multiplexed transdermal detection of metabolites” and also previous research performed in the lab, such as the method used for glucose detection [15] [23].

Penetration Force Experiment

Mechanical strength testing of the MNAs were conducted using a force gauge device. MNAs were inserted into 3 wt% agarose hydrogel and the alterations in penetration force relative to displacement were recorded. It was concluded that the MN design was sharp enough to penetrate skin-models and that it could be used for ISF based detection and drug delivery.

Scratch Wound Healing Assay and Cell Viability Assay

To study the performance of the ultrasonic-assisted drug delivery MNA set, a scratch test experiment was conducted. A scratch was created on a layer of keratinocyte cells adhered in a 24-well plate, using a fine micropipette tip. Three samples were prepared: one with 2 vol.% of B27 supplement added using an ultrasonic-assisted MNA, another with 2 vol.% of B27 supplement added directly to the media, and a third without any B27 supplement as a control. The scratch was monitored using bright field images taken after 1 and 2 days.

To assess the cell viability of the experimental samples, an indirect extraction approach was employed. The 3D printed MNAs were incubated in triplicate for 24 hours in 5 mL of Dulbecco's Modified Eagle Medium (DMEM) with 10% v/v fetal bovine serum (FBS) at 37 °C, under 5% CO2, and in a fully humidified air environment. Following a 24-hour incubation of 3D printed MNAs in the media, 400 µL of the extracted media was transferred into each well of 24-well plates, with 100,000 cells per well. The Presto Blue (PB) assay, a standard method for rapidly evaluating the viability and proliferation of various cell types, was employed by tracking the metabolic activity of live cells. Subsequently, the samples were allowed to incubate for 24 and 48 hours. The metabolic activity of the cells was assessed using a PB cell viability reagent. A 100 µL solution of 10% PB reagent in DMEM was prepared and added to each well at both time points. The plate was then incubated for 15 minutes, and the fluorescent intensity of the cells was measured with excitation and emission wavelengths set at 560 nm and 590 nm, respectively.

The formula described below was then applied to calculate the viability of the samples:

Cell Viability: (Average fluorescent density of the samples/Average fluorescent density of the control) $*$ 100.

Smartphone-Enabled Sensing

A smartphone application was created for colorimetric analysis using a sensing compartment. The detection MNA has a 2 x 2 quadrant view section where up to 4 test paper strips can be loaded. The user begins by capturing a photo of the paper strip loaded onto the detection microneedle with the smartphone camera. The paper strip changes color based on the concentration of the biomarker in ISF. This is facilitated as capillary forces suck skin ISF through the holes in the MNA thereby wetting the test strip. Subsequently, the cropped portion of the image taken is imported onto the analysis interface of the application. The application then computes the average RGB values of the test paper photo and accurately presents these values, along with a picture of the corresponding average color for better visualization and visual confirmation. This averaging approach is employed to address the non-uniform characteristics of the colored area on the test strips and to accommodate for variation in lighting conditions in the real world. Following this, the application

utilizes idealized percentage RGB curves associated with biomarkers based on curve fitting data collected to determine and exhibit the concentrations of these biomarkers. Thus, a user of the microneedle wearable device can with ease, monitor the three biomarkers that were tested for which are glucose, pH and lactate.

Smartphone-Enabled Drug-Delivery

To enable wireless drug delivery on demand, a specialized electronic module was created to power the ultrasonic membrane responsible for facilitating drug release within the drug delivery compartment. Initial tests to check the working of the membrane was performed with commercially available power modules that are powered on by a DC 5V source. Furter tests were done using the custom power module. The electronic module is composed of an Arduino Nano microcontroller, a motor driver module, a low-energy Bluetooth module, and a battery. A smartphone application is employed to initiate the ON/OFF mechanism, utilizing terminal commands of 1/0 to activate or deactivate the pump. Upon receiving an ON command from the app via the Bluetooth module, the Arduino microcontroller generates analog outputs in the form of a square wave signal. This signal causes the ultrasonic membrane to vibrate at 113 kHz, thereby propelling the drug as a mist through the membrane and subsequently through the MNA holes. Conversely, upon receiving an OFF command, the microcontroller ceases sending the signal, causing the membrane to stop vibrating and consequently halting the drug flow. Custom settings are set in the user interface for various timed releases of the drug. Thus, the patient themselves or their doctor can trigger timely drug delivery on-demand. An added advantage of the custom power module for the drug delivery ultrasonic membrane is its versatility. In addition to enabling Bluetooth-based wireless remote control, it can be adapted in the future to support wearable devices utilizing membranes with varying natural frequencies. It can also be modified to work with multiple membranes thus allowing the delivery of multiple drugs. The safety and biocompatibility of PEGDA ensures that the MNA device can be used for an extended period.

RESULTS AND DISCUSSION

Fabrication of MNAS

The MNAs in the study were manufactured using digital light processing (DLP) 3D printing technique. The DLP printing process used for making the MNAs is illustrated in Figure 6B. To assess the printability of the MNAs, two categories (sensing and drug delivery sets) were 3D printed. Computer-aided design (CAD) software was employed to create the 3D model of both sets of MNAs (4 by 4). Digitally, the 3D model underwent slicing into numerous cross-sectional images in the slicing software. Each digital image was then transmitted to a Digital Micromirror Device (DMD), generating patterned light (405 nm), which was subsequently directed through a projection lens and focused onto the surface of the photosensitive precursor solution. The projected light caused the liquid photosensitive precursor solution to solidify into a structured layer. To form a 3D MNA, this layering process was iteratively performed.

In this investigation, polyethylene glycol diacrylate (PEGDA) was used, with a molecular weight of 250 Daltons (PEGDA 250) as the monomer, phenylbis(2,4,6-trimethylbenzoyl)-phosphine oxide (Irgacure 819) as a photoinitiator, and Sudan I as a photoabsorber to formulate the bioink. We printed the MNAs with a tilt angle of 45 °C along one axis, a configuration determined by previous research conducted by our team to enhance tip sharpness and the penetration ability of MNAs (It must be noted that two axes tilt provides improved tip sharpness, but it may result in the needle lumens being clogged for hollow MNAs. Thus, two-axis tilt is recommended for 3D printing solid and coated MNAs). Figure 6C illustrates the smartphone control enabled system for sensing and drug delivery compartments respectively, and Figures 6D and 6E depict the SEM images of 3D printed MNA.

As mentioned before, the MNA system in this study had two compartments: 1) biosensing and 2) drug delivery. The biosensing compartment was made in the form of a square with shape and dimensions shown in Figure 7A. A sensing window was then designed to house paper-based colorimetric sensor array for quantifying glucose, pH, and lactate. The drug delivery compartment was designed in the form of a cylinder that housed an ultrasonic vibrator that atomized drug solutions and delivered them into tissue *via* hollow microneedles. An inlet port was designed to refill the drug chamber. For the assessment of characteristics and experimentation in the study, MNAs for both sensing and drug delivery were designed and manufactured, with dimensions and shapes depicted in Figures 7A, 7B, and 7C. It must be noted that for this study a 4x4 array of MNAs were used as a proof of concept for drug delivery and biomarker detection. However, the number of needles can be optimized for specific applications. As the array has a small footprint, such an addition or subtraction can easily be accommodated.

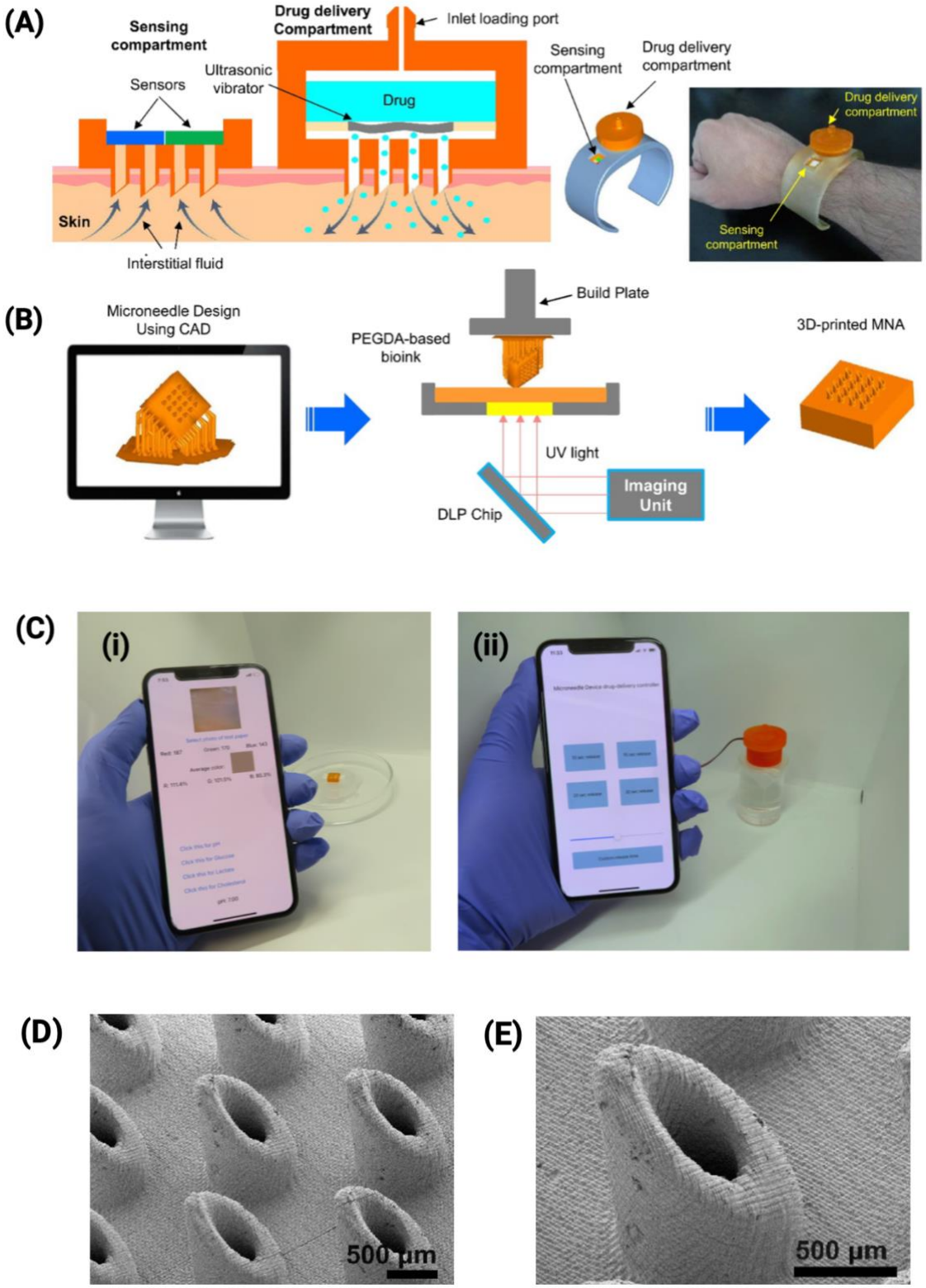

Figure 6: (A) Concept of the developed device in this research; (B) Schematic illustration of the fabrication process of MNAs; (C) Smartphone enable control on (i) Sensing, and (ii) Drug delivery; (D) SEM image of 3D printed MNA; (E) SEM image of 3D printed MN seen with higher magnification [20].

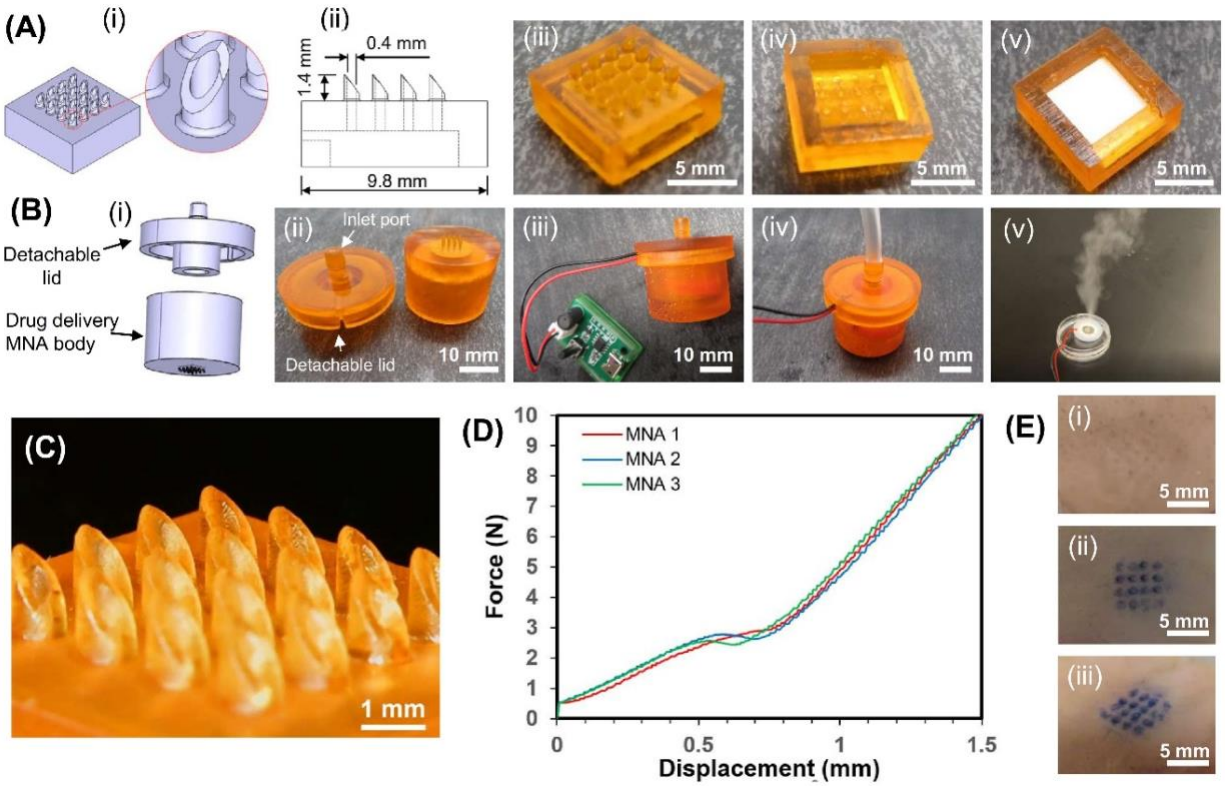

Figure 7: Images of 3D printed sensing and drug delivery MNAs; (A) Sensing MNA, (i, ii) 3D model and needle dimensions, (iii) View from needles' side, (iv) View from sensor side, (v) View from sensor side with a paper sensor (B) Drug delivery MNA, (I, ii, iii) 3D model of the set including body and cap parts, (iv) 3D printed body and cap parts, (v) Whole set including ultrasonic atomizer and power module, (vi) Attached tubing for charging the drug in the reservoir; (C) Optical image of the 3D printed needles; (D) Force-displacement graph for the mechanical testing of MNAs; (E) Pig skin penetration of MNAs, (i) Pig skin after penetration of MNA, without blue die, (ii) Top view of pig skin after penetration of MNA with a blue dye, (iii) pig skin after penetration of MNA with a blue dye [20].

Mechanical Strength and Penetration Testing

Good mechanical properties that are sufficient to penetrate the skin are one of the main requirements when using MNAs for various applications. A compression mechanical testing system was used to determine the required force for MNA penetration in a 3 wt% agarose hydrogel and the changes in penetration force against displacement were measured. This method was exactly similar to previous research work done in LiME, to study the effect of tilt-angle 3D printing MNAs on its penetration capability [105]. Basic mechanical testing of the MNAs was conducted using a force gauge and a custom-made compression test device, to assess the penetrating capability into skin models. Figure 7D shows the force-displacement graph for the mechanical

testing. As can be seen, the force needed for the penetration of three different MNAs is comparatively the same. The force required for the penetration of three distinct MNAs remains consistently ≈3 N. Examining the force-displacement graph, it becomes apparent that the force applied does not result in the failure of MNA even as it increases post-penetration. This trend is indicative of the safety and robustness of using these microneedles. In addition, the MNA was evaluated by penetrating pig skin to assess its performance in skin penetration. Figure 7E also shows the pig skin before and after MNA insertion using blue dye. The outcomes of the penetration test conducted on pig skin demonstrated that the 3D-printed MNA effectively penetrated skin. However, hollow MNAs are notoriously prone to breakage and design modifications in terms of geometry, materials, post-treatment and maintenance routines may be necessary for animal or human trials. For the scope of this experiment, based on the mechanical strength and chance of breaking, the optimized design was deemed safe.

Sensing

In this study, we utilized 4x4 needle MNAs for sensing, illustrated in Figures 8A and 8B. Figure 8A represents the MNA designed for individual biomarker sensing, while Fig 8B illustrates the MNA designed for simultaneous sensing of various biomarkers. It includes a colorimetric sensor paper as shown in the photos.

Initially, for optimization purposes, we investigated how the hole diameter of MNAs affects their sensing performance. MNAs with hole diameters of 0.4, 0.8, and 1.2 mm (400, 800, and 1200 µm) were designed and 3D-printed, and their sensing properties were subsequently characterized. It's worth noting that a hole diameter of 400 µm in an MNA can be achieved with an affordably priced DLP printer. It must be noted that as our work served as a proof-of-concept, some dimensions may not reflect the practical scale of a microneedle that is suitable for animal or clinical trials. The exact geometry of a MNA that is suitable for live animal and clinical trials is something that needs to be optimized in future work. The minimum diameter achievable with our low-cost 3D printer was 400 µm, as this yields a reliable and smooth cylindrical lumen, and other diameters were chosen to ensure the impact of hole size could be observed in the test results, such as a reduction in capillary force induced rise of model skin ISF with an increase in hole diameter. Based on the results, as shown in Figure 8C, MNA with 400 µm diameter had the best performance for the sensing. In this experiment, an increase in wetted area, which could be an index for the sensing rate, in MNA with 0.4 mm hole diameter MNA is much higher than that of MNAs with 0.8 mm and 1.2 mm hole diameter MNA, indicating that a decrease in hole diameter can increase the sensing rate. Based on these results, we selected 400 µm as the hole diameter of MNAs for this research.

The process by which the solution reaches the sensor paper relies on capillary force. Tests were performed with biomarker loaded in DI water with resulted in test paper wetting, and as skin ISF has viscosity comparable to that of water [106], it can be assumed that it will yield the same results. To check the response time of MNA's sensing, we monitored the changes in the sensor paper's wetted area. As can be seen in Figure 8D, the MNA's response time is about 4 min which seems very reasonable. As observed from Figure 8A and pictures at the bottom of graph 8D corresponding to 30 second intervals starting from 0 seconds, about 4 minutes is the time that is required for complete wetting of the test paper, where the x and y axes represent wetted area and time respectively. It was also observed that once wetting starts, within a matter of seconds the entire test strip is wet. However, this does not account for the additional time that is required for the chemical reaction that needs to occur to observe a color change. For pH, it is the time required for bromocresol green to change color, which is observed within a matter of seconds. For glucose and lactate, the time required for oxidase-peroxidase reaction, followed by the redox reaction involving a chromogenic dye which yields a color change- varies significantly based on biomarker concentration and it can take up to a few minutes to stabilize. Therefore, additional time is required and recommended to perform RGB analysis of the test strips. To recap, the sensing capabilities of the microneedle arrays (MNAs) were assessed by measuring three biomarkers: pH, glucose, and lactate.

Monitoring physiological pH is particularly crucial in clinical settings as it provides insights into the body's regulatory systems. Even a slight deviation in physiological pH can impact cellular, tissue, and organ functions, making it a valuable early sensing tool for diseases. Monitoring pH levels in both tissues and organs is essential for diagnosing various diseases. In this research, MNAs successfully demonstrated colorimetric detection of pH levels ranging from 3 to 8, as this is a physiologically relevant range. Figure 8E illustrates representative images depicting the color changes in the MNA sensor corresponding to different pH values, along with the associated variations in red, green, and blue (RGB) percentages, ranging from 3 to 8 [20].

Typical fasting blood glucose levels range from 3.9 to 6.1 mM and may increase to 7.9 mM two hours after a meal in individuals with good health. For diabetic patients, plasma glucose levels that surpass 7.0 mM on an empty stomach or 11.1 mM on a 2-hour post-prandial test are indicative of their condition. Effectively managing diabetes relies on the timely monitoring of fluctuating blood glucose levels. However, the conventional method of blood testing through finger-pricking is not practical for frequent use due to poor patient compliance. An alternative, painless, and bloodless approach involves the use of microneedles. Here, MNAs were employed to measure glucose concentrations ranging from 0 to 16 mM. Figure 8F illustrates the variations in RGB percentages corresponding to glucose concentrations between 0 to 16 mM, as detected by MNAs [20].

The blood lactate level is influenced by oxygen supply and metabolism, serving as a biomarker for assessing the severity of conditions like acute carbon monoxide poisoning, sepsis, neonatal asphyxia, trauma, and acute hemorrhagic shock. Timely sensing of lactate is crucial for monitoring

patients in critical conditions. Typically, normal blood lactate concentration ranges from 0.5 to 1.7 mM at rest, with a modest increase after exercise. Hyperlacticaemia, characterized by levels exceeding 2 mM, particularly impacts tissues and organs with high metabolic rates, leading to manifestations such as muscle weakness and hepatic failure. Figure 8G shows changes in RGB percent for lactate concentrations between 0 to 3.2 mM [20].

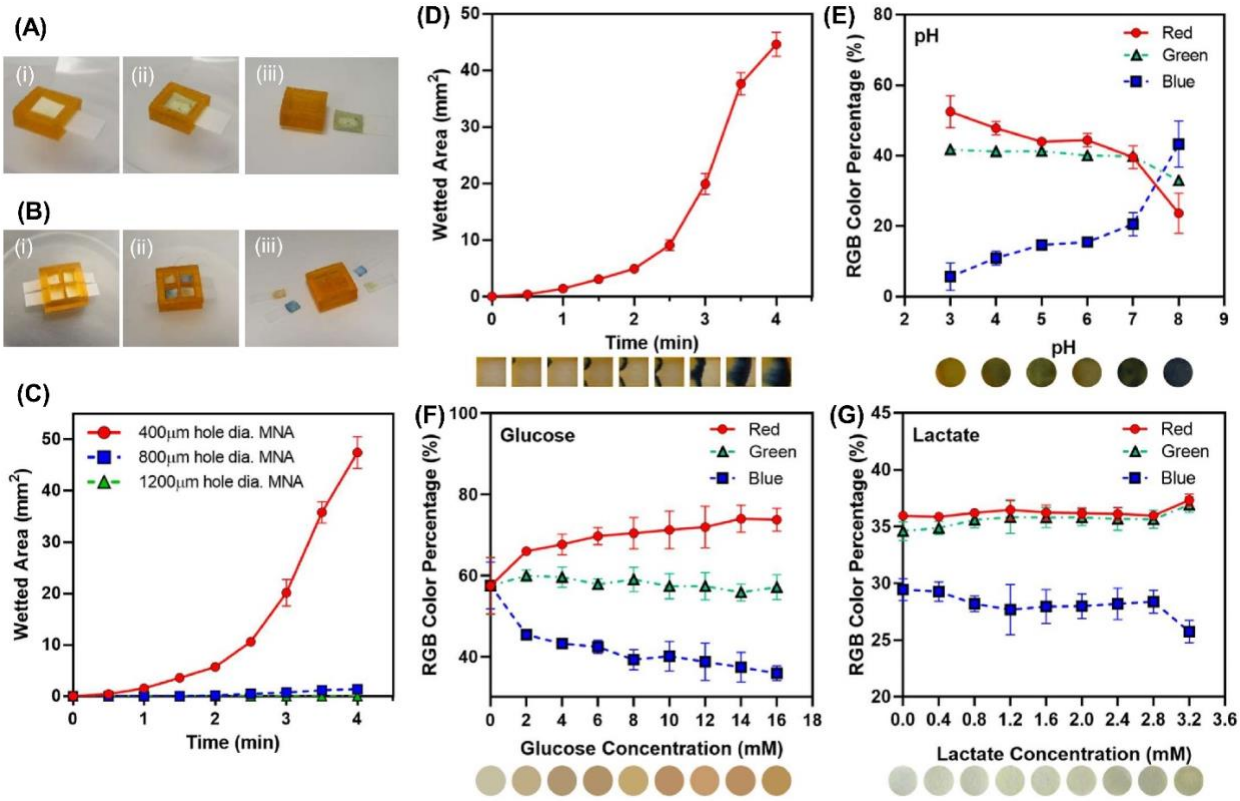

Figure 8: (A) MNA for individual biomarker sensing; (B) MNA designed for simultaneous sensing of various biomarkers; (C) Effect of hole diameter on sensing showing the changes of the sensor wetted area against time for MNAs with 0.4, 0.8, and 1.2 mm hole diameters; (D) changes of the sensor paper's wetted area against time as an index for MNA's response time. Changes of RGB percent for biomarkers detected with MNAs (E) pH ranging from 3 to 8; (F) glucose with 0 to 16 mM concentrations; (G) lactate with 0 to 3.2 mM concentrations [20].

Drug Delivery

To compare the drug delivery rate through topical use, using microneedle, and using ultrasonic-assisted microneedle, an experiment using a Franz cell chamber was carried out. In this experiment, a layer of Parafilm® was used as the membrane. Parafilm® has been used extensively in earlier work as a skin simulant in in vitro tests [107] [108] [109]. Although not an exact replacement for human or animal skin, for the scope of this experiment it served as a barrier and separator for the MNA base and fluid. The chamber was filled with DI water to act as the region where drug would be delivered. Figures 9A and 9B show the set-up used for this experiment.

Figure 9C reveals the comparative drug delivery results. As can be seen, the drug delivery rate in the ultrasonic-assisted MNA condition is much higher than topical and microneedle conditions while the microneedle had a much better drug delivery rate than the topical condition. Thus, we concluded that the ultrasonic-assisted membrane was a successful method to deliver model drugs into ISF.

In another experiment, to study the effect of MNA's hole diameter on the drug delivery application, optimized MNA with 400 µm lumen diameter was compared with MNAs with 200 µm, 300 µm, and 500 µm lumen diameter MNAs. As it was needed to make MNAs with lumens smaller than 400 µm with a resolution higher than the ordinary one, we used a Micro 3D printer to make MNAs with 200 µm, 300 µm, and 500 µm lumens to compare them. The results showed that increasing the lumen diameter can increase the drug delivery rate as shown in Figure 9D. So, it shows that is possible to control the drug delivery rate by using different MNA hole diameters. However, the optimized 400 µm lumen diameter was sufficient for all model drugs tested and controlling the flow rate through the ultrasonic membrane was deemed a better way to control drug delivery rates. This can very easily be achieved by controlling the time-period for which the device is switched on.

To show that the drug delivery rate could be controlled on demand, we performed ON and OFF cycles by powering the ultrasonic atomizer for 1 minute in 30-minute intervals. The model drug used was Rhodamine B. It must be noted that most of the drug for the fixed dose selected, is delivered in under a minute and a longer on time ensures that the rest of the drug is delivered. The outcomes of this experiment are shown in Figure 9E. As observed, the drug delivery rate could be controlled using an ON-OFF procedure. Additionally, the evaluation included an assessment of the smartphone-controlled system for on-demand drug delivery. The findings indicated that the system successfully managed wireless on-demand drug delivery. Figure 9F illustrates the various stages of this experiment. The efficiency of drug delivery for each ON cycle was not studied. However, from figure 9E, it can be observed from the step nature of the graph that each ON cycle is able to deliver a near consistent amount of drug. Thus, it can be concluded that ultrasonic membrane assisted drug delivery holds potential in being a high efficiency method which holds promise as an alternative to hypodermic needle injection.

Moreover, to demonstrate the effectiveness of the ultrasonic-assisted MNA drug delivery approach, an experiment was carried out using a hydrogel block. The MNA successfully penetrated the hydrogel, and drug delivery was facilitated by the ultrasonic membrane. Figure 9G depicts various images associated with this test. The color change of the hydrogel block as observed from figure 9G images (i)- (vi), demonstrates that the drug delivery component of the device can successfully deliver model drugs into hydrogel model skin.

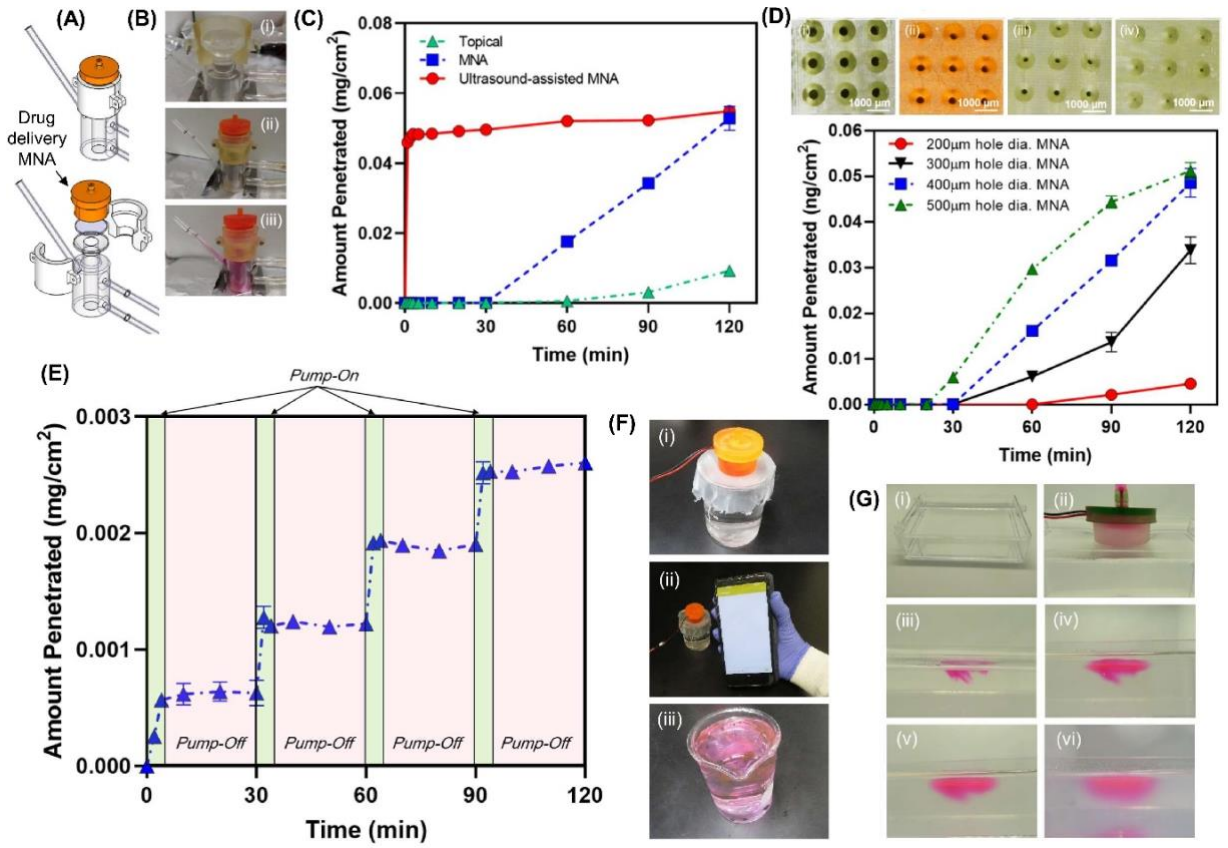

Figure 9: (A) A schematic showing the Franz Cell set used for the drug delivery experiment; (B) Actual Franz Cell drug delivery set, (i) A view showing the components of the set, the set (ii) before and (iii) after drug delivery; (C) Compare of drug delivery on topical, MNA, and ultrasonic-assisted MNA drug delivery methods; (D) Compare of drug delivery for MNAs with (i) 500µm, (ii) 350 µm, (iii) 300 µm, (iii) 200 µm; (E) The graph showing the ON-OFF drug delivery control; (F) Smartphone control enabled drug delivery, (i) before drug delivery, (ii) Start of drug delivery using the app, and (iii) After drug delivery; (G) Ultrasonic-assisted MNA drug delivery into the hydrogel block (i) hydrogel block before the test, (ii) Drug delivery set penetrated the hydrogel before the drug delivery, (iii) hydrogel 5 minutes after starting the drug delivery, (iv) hydrogel 10 minutes after the drug delivery, (v) hydrogel 1 h after starting the drug delivery, (vi) hydrogel 6 h after starting the drug delivery [20].

Scratch Test and Cytotoxicity

To test how well the ultrasonic-assisted MNA can deliver real drugs to skin, we conducted a scratch test experiment. We created a scratch on a layer of keratinocyte cells using a fine micropipette tip. To promote cell growth, we added the B27 supplement, known to be effective for cell growth. Three samples were prepared: one with 2 vol.% of B27 supplement added using an ultrasonic-assisted MNA, another with 2 vol.% of B27 supplement added directly to the media, and a third without any B27 supplement as a control. In this study, we aimed to compare the drug delivery device performance with the condition when added directly to the media. We monitored the scratch area using bright field images taken after 1 and 2 days. The results, shown in Figures 10A, 10B, and 10C, indicate that the ultrasonic-assisted MNA performed similarly to adding the supplement directly. This suggests that the device can effectively delivers real drugs to skin cells.

Materials like the ones examined in this study have found application in MNAs for drug delivery and have been generally considered non-cytotoxic. Despite their established safety, evaluating their cytotoxicity at relevant concentrations is crucial to ensure their suitability for medical research and clinical use. A cell viability assay was conducted following the ISO-10993 standard to assess the cytotoxicity of the devices. The results from the experiments indicated that the tested material is suitable for making MNAs for drug delivery and sensing applications. As illustrated in Figure 10D, the decline in cell viability after 24, and 48 h was deemed not statistically significant when compared to the first day of incubation. Thus, the materials used in the device were concluded to be biocompatible for skin cell exposure for extended periods of time.

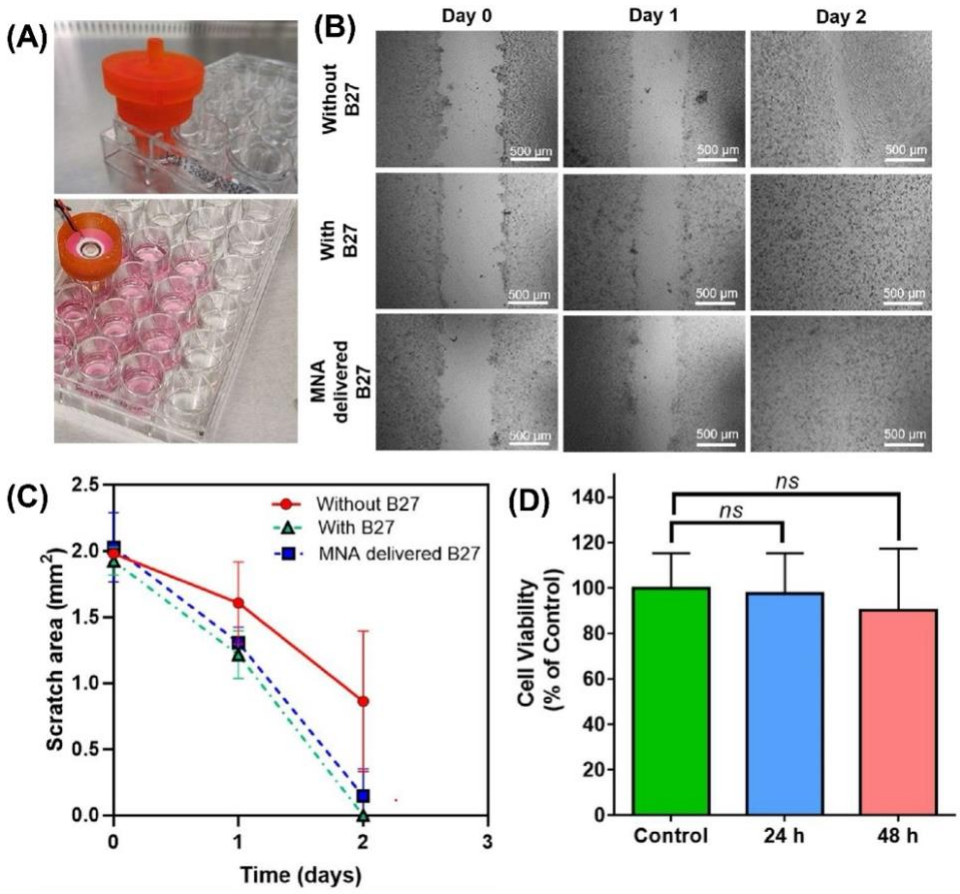

Figure 10: (A) The drug-delivery setup used for the scratch test assay; (B) Bright-field images of the scratch area at the start of the test and after 1, and 2 days; (C) Scratch area changes against time for different conditions; (D) Cell viability test results [20].

CONCLUSION

This study explores the potential of a device having 3D-printed hollow MNAs for biomarker sensing and on-demand drug delivery. The investigation focuses on the fabrication, characterization, and performance evaluation of the proposed device set for both the sensing and drug delivery components. The dual functionality of colorimetric monitoring of biomarkers and on-demand drug delivery presents a versatile and innovative approach to closed-loop on-demand drug delivery. The fabrication process utilizing DLP printing with polyethylene glycol diacrylate (PEGDA) as a monomer showcases the adaptability of 3D printing in creating intricate structures with precise control over geometry. The MNAs, designed with a 45-degree tilt angle, demonstrate maintained structural integrity upon 3D printing. The choice of a 400 µm lumen/hole diameter for sensing MNAs is justified by its superior performance in terms of wetted area and sensing rate. The same lumen diameter can be used for the drug delivery MNA as the amount of drug delivered can be controlled by turning the pump ON/OFF as required. A timed release also ensures that a certain dose of drug is delivered.

The sensing capabilities of the MNAs are demonstrated through colorimetric analysis of three key biomarkers viz.- pH, glucose, and lactate. The results showed promising response times and sensitivity, emphasizing the potential for real-time monitoring of physiological parameters using this device. The ability to detect biomarkers in skin ISF provides a near-painless, non-invasive and alternative to traditional blood-based diagnostics. Furthermore, the drug delivery aspect of the device is evaluated through comparative studies involving topical application, microneedle penetration, and ultrasonic-assisted microneedle delivery. The ultrasonic-assisted microneedle approach proves significantly more effective in drug delivery compared to the other methods, showcasing the potential for controlled and enhanced drug administration. The study delves into the impact of MNA hole diameter on drug delivery rates, highlighting the importance of customization for specific applications. Additionally, a scratch test assay demonstrates the effectiveness of ultrasonic-assisted MNAs in delivering drugs for promoting cell growth, suggesting potential applications in wound healing. Mechanical testing of MNAs confirmed the safety and durability of the MNAs, indicating their resilience to forces applied during penetration without failure.

Some of the disadvantages of the device are listed as follows. Firstly, there is a limit on the resolution that can be achieved with a DLP 3D printer. Although tip sharpness can be improved with tilt-angle fabrication. It still may not be sharp enough for clinical applications. Traditional hypodermic needles are made using tube drawing and have an extremely sharp tip and have proven its place for drug delivery and diagnostics. Moreover, stainless steel is significantly stronger and robust than plastics. So, achieving mechanical performance comparable to hypodermic needles may take many iterations of design improvements. Secondly, the detection method is proposed to

be an affordable alternative for diagnostics. Colorimetric sensors have been used for a wide variety of diagnostics applications. The coated filter paper strip is affordable to produce in a laboratory setting, thus it must be even more affordable to mass produce. But there is a notable inconsistency in color distribution within the paper once in has been soaked by biomarker loaded liquid. The application developed can average out the color and accommodates for this- to an extent. But an optimized strip material is recommended. Also, optimizing the coating process in terms of methods can yield a significantly higher accuracy in accurately quantifying the biomarker concentration. A larger data set is required to yield a more accurate calibration curve. But an added advantage is that, since the strips are colorimetric sensors, visual detection based on a reference sheet can be used to verify biomarker concentration. However, the time required for color change for each biomarker is different, ranging from a few seconds to a few minutes. Although this is a lot higher than blood sampling and testing in a lab, it is not inherently better than commercially available and proven devices such as glucose meters. Furthermore, although the device itself is reusable, the test strips are single-use sensors and must be discarded after use. Therefore, a test strip cannot provide a continuous readout on variation in biomarker concentration. Further work must be performed to investigate potential colorimetric sensors that can dynamically change color for continuous use. Additionally, further work must be performed to check the biocompatibility of the reagents used to make the test strips as it can potentially leak into skin ISF, causing infection or toxicity.

For drug delivery, there is a limit on the amount of drug that can be delivered into ISF before saturation compared to intravenous drug delivery. There is also the possibility of drugs being underdelivered, as some of the drug can be stuck within the drug loading chamber or within the silicone shield of the ultrasonic membrane. The experiments performed were using small molecules and it is possible that larger molecules may be difficult to be delivered using this method. Drug delivery is also limited by the pore size of the ultrasonic membrane. Furthermore, not all drugs are soluble in ISF compatible solvents. This aspect needs to be investigated using real drugs that are typical for chronic diseases.

Subsequently, further work in this filed can result in MNA based detection methods for more physiologically relevant biomarkers that are typical for patients with chronic diseases. It can also lead to more optimized drug-delivery for real drugs on-demand utilizing MNA based systems.

The proposed concept-wearable-device fabricated using DLP-3D printing and utilizing hollow MNAs presents a multifaceted solution for health monitoring and on-demand drug delivery. The combination of 3D printing technology, biomarker sensing, and ultrasonic-assisted drug delivery opens new possibilities for personalized and patient-friendly healthcare solutions. Further research and development in this direction hold promise for addressing challenges in drug adherence and improving quality of care for chronic disease treatment.

WORKS CITED

[1] R. H. Shmerling, "Terrified of needles? That can affect your health," Harvard Health Publishing, 27 April 2021. [Online]. Available: https://www.health.harvard.edu/blog/terrified-of-needles-that-can-affect-your-health-2021042722470.

[2] G. Smyth, "Needle phobias are preventing some people from getting COVID-19 vaccines. These interventions could help," CBC News, 3 November 2021. [Online]. Available: https://www.cbc.ca/news/health/needle-phobia-prevention-1.6229655.

[3] J. Yang, X. Liu, Y. Fu and Y. Song, "Recent advances of microneedles for biomedical applications: drug delivery and beyond," *Acta Pharmaceutica Sinica B,* vol. 9, no. 3, pp. 469-483, 2019.

[4] M. M. Phillips, D. C. Dugdale, B. Conaway and A. E. team, "Drug-induced liver injury," National Library of Medicine, 31 October 2022. [Online]. Available: https://medlineplus.gov/ency/article/000226.htm#:~:text=Nonsteroidal%20anti%2Dinflammatory%20drugs%20(NSAIDs,Anabolic%20steroids.

[5] P. Rajpurkar, E. Chen, O. Banerjee and E. J. Topol, "AI in health and medicine," *Nature Medicine,* vol. 28, p. 31–38, 2022.

[6] F. M. Iqbal, K. Lam, M. Joshi, S. Khan, H. Ashrafian and A. Darzi, "Clinical outcomes of digital sensor alerting systems in remote monitoring: a systematic review and meta-analysis," *NPJ Digit Med,* vol. 4(1), no. 7, 2021.

[7] A. N. Navaz, M. A. Serhani, H. T. E. Kassabi, N. Al-Qirim and H. Ismail, "Trends, Technologies, and Key Challenges in Smart and Connected Healthcare," *IEEE Access,* vol. 9, p. 74044–74067, 2021.

[8] J. Choi, D. Kang, S. Han, S. B. Kim and J. A. Rogers, "Thin, Soft, Skin-Mounted Microfluidic Networks with Capillary Bursting Valves for Chrono-Sampling of Sweat," *Advanced Healthcare Materials,* vol. 6, no. 5, 2017.

[9] W. Gao, S. Emaminejad, H. Y. Y. Nyein, S. Challa, K. Chen, A. Peck, H. M. Fahad, H. Ota, H. Shiraki, D. Kiriya, D.-H. Lien, G. A. Brooks, R. W. Davis and A. Javey, "Fully integrated wearable sensor arrays for multiplexed in situ perspiration analysis," *Nature,* vol. 529, p. 509–514, 2016.

[10] S. Niu, N. Matsuhisa, L. Beker, J. Li, S. Wang, J. Wang, Y. Jiang, X. Yan, Y. Yun, W. Burnett, A. S. Y. Poon, J. B.-H. Tok, X. Chen and Z. Bao, "A wireless body area sensor network based on stretchable passive tags," *Nature Electronics,* vol. 2, p. 361–368, 2019.

[11] J. Zhang, J. Xu, J. Lim, J. K. Nolan, H. Lee and C. H. Lee, "Wearable Glucose Monitoring and Implantable Drug Delivery Systems for Diabetes Management," *Advanced Healthcare Materials,* vol. 10, no. 17, 2021.

[12] J. Li, J. Y. Liang, S. J. Laken, R. Langer and G. Traverso, "Clinical Opportunities for Continuous Biosensing and Closed-Loop Therapies," *Trends in Chemistry,* vol. 2, no. 4, pp. 319-340, 2020.

[13] P. L. Mage, B. S. Ferguson, D. Maliniak, K. L. Ploense, T. E. Kippin and H. T. Soh, "Closed-loop control of circulating drug levels in live animals," *Nature Biomedical Engineering,* vol. 1, 2017.

[14] M. Dervisevic, E. Dervisevic, L. Esser, C. D. Easton, V. J. Cadarso and N. H. Voelcker, "Wearable microneedle array-based sensor for transdermal monitoring of pH levels in interstitial fluid," *Biosensors and Bioelectronics,* 2023.

[15] D. D. Zhu, L. W. Zheng, P. K. Duong, R. H. Cheah, X. Y. Liu, J. R. Wong, W. J. Wang, S. T. T. Guan, X. T. Zheng and P. Chen, "Colorimetric microneedle patches for multiplexed transdermal detection of metabolites," *Biosensors and Bioelectronics,* 2022.

[16] S. R. Dabbagh, M. R. Sarabi, R. Rahbarghazi, E. Sokullu, A. K. Yetisen and S. Tasoglu, "3D-printed microneedles in biomedical applications," *iScience,* vol. 24, no. 1, 2020.

[17] S. Dharadhar, A. Majumdar, S. Dhoble and V. Patravale, "Microneedles for transdermal drug delivery: a systematic review," *Drug Development and Industrial Pharmacy,* vol. 45, no. 2, pp. 188-201, 2019.

[18] S. Mdanda, P. Ubanako, P. P. D. Kondiah, P. Kumar and Y. E. Choonara, "Recent Advances in Microneedle Platforms for Transdermal Drug Delivery Technologies," *Polymers,* vol. 13, no. 15, 2021.

[19] H. Chang, M. Zheng, X. Yu, A. Than, R. Z. Seeni, R. Kang, J. Tian, D. P. Khanh, L. Liu, P. Chen and C. Xu, "A Swellable Microneedle Patch to Rapidly Extract Skin Interstitial Fluid for Timely Metabolic Analysis," *Advanced Materials,* vol. 29, no. 37, 2017.

[20] M. Razzaghi, J. A. Ninan, M. Azimzadeh, E. Askari, A. H. Najafabadi, A. Khademhosseini and M. Akbari, "Remote-Controlled Sensing and Drug Delivery via 3D-Printed Hollow Microneedles," *Advanced Healthcare Materials,* 2024.

[21] M. T. C. McCrudden, E. McAlister, A. J. Courtenay, P. González-Vázquez, T. R. R. Singh and R. F. Donnelly, "Microneedle applications in improving skin appearance," *Experimental Dermatology,* vol. 24, no. 8, pp. 561-566, 2015.

[22] Z. Sartawi, C. Blackshields and W. Faisal, "Dissolving microneedles: Applications and growing therapeutic potential," *Journal of Controlled Release,* vol. 348, pp. 186-205, 2022.

[23] M. Razzaghi, A. Seyfoori, E. Pagan, E. Askari, A. H. Najafabadi and M. Akbari, "3D Printed Hydrogel Microneedle Arrays for Interstitial Fluid Biomarker Extraction and Colorimetric Detection," *Polymers,* vol. 15, no. 6, 2023.

[24] M. Avcil and A. Çelik, "Microneedles in Drug Delivery: Progress and Challenges," *Micromachines (Basel),* vol. 12, no. 11, 2021.

[25] Y.-C. Kim, J.-H. Park and M. R. Prausnitz, "Microneedles for drug and vaccine delivery," *Advanced Drug Delivery Reviews,* vol. 64, no. 14, pp. 1547-1568, 2012.

[26] T. Waghule, G. Singhvi, S. K. Dubey, M. M. Pandey, G. S. Gupta, M. Singh and K. Dua, "Microneedles: A smart approach and increasing potential for transdermal drug delivery system," *Biomedicine & Pharmacotherapy,* vol. 109, pp. 1249-1258, 2019.

[27] U. Detamornrat, M. Parrilla, J. Domínguez-Robles, Q. K. Anjani, E. Larrañeta, K. D. Wael and R. F. Donnelly, "Transdermal on-demand drug delivery based on an iontophoretic hollow microneedle array system," *Lab On a Chip,* vol. 23, no. 9, pp. 2304-2315, 2023.

[28] Y. Li, H. Zhang, R. Yang, F. Tazrin, C. Zhu, M. Kaddoura, E. J. Blondeel and B. Cui, "In-plane silicon microneedles with open capillary microfluidic networks by deep reactive ion etching and sacrificial layer based sharpening," *Sensors and Actuators A: Physical,* vol. 292, pp. 149-157, 2019.

[29] H. Kathuria, K. Kang, J. Cai and L. Kang, "Rapid microneedle fabrication by heating and photolithography," *International Journal of Pharmaceutics,* vol. 575, 2020.

[30] Z. F. Rad, R. E. Nordon, C. J. Anthony, L. Bilston, P. D. Prewett, J.-Y. Arns, C. H. Arns, L. Zhang and G. J. Davies, "High-fidelity replication of thermoplastic microneedles with open microfluidic channels," *microsystems & nanoengineering,* vol. 3, 2017.

[31] H. R. Nejad, A. Sadeqi, G. Kiaee and S. Sonkusale, "Low-cost and cleanroom-free fabrication of microneedles," *microsystems & nanoengineering,* vol. 4, 2018.

[32] J. Li, B. Liu, Y. Zhou, Z. Chen, L. Jiang, W. Yuan and L. Liang, "Fabrication of a Ti porous microneedle array by metal injection molding for transdermal drug delivery," *PLoS One,* vol. 12, no. 2, 2017.

[33] R. F. Donnelly, R. Majithiya, T. R. R. Singh, D. I. J. Morrow, M. J. Garland, Y. K. Demir, K. Migalska, E. Ryan, D. Gillen, C. J. Scott and A. D. Woolfson, "Design, optimization and characterisation of polymeric microneedle arrays prepared by a novel laser-based micromoulding technique," *Pharmaceutical Research,* vol. 28, no. 1, pp. 41-57, 2011.

[34] J. Wang, H. Wang, L. Lai and Y. Li, "Preparation of Microneedle Array Mold Based on MEMS Lithography Technology," *Micromachines,* vol. 12, no. 1, 2021.

[35] J. Lim, D. Tahk, J. Yu, D.-H. Min and N. L. Jeon, "Design rules for a tunable merged-tip microneedle," *microsystems & nanoengineering,* vol. 4, 2018.

[36] M. Ogundele and H. K. Okafor, "Transdermal Drug Delivery: Microneedles, Their Fabrication and Current Trends in Delivery Methods," *Journal of Pharmaceutical Research International,* vol. 18, no. 5, pp. 1-14, 2017.

[37] S. N. Economidou, M. J. Uddin, M. J. Marques, D. Douroumis, W. T. Sow, A. Reid, J. F. Windmill and A. Podoleanu, "A novel 3D printed hollow microneedle microelectromechanical system for

controlled, personalized transdermal drug delivery," *Additive Manufacturing,* vol. 38, no. 101815, 2020.

[38] A. R. Johnson and A. T. Procopio, "Low cost additive manufacturing of microneedle masters," *3D Printing in Medicine,* vol. 5, no. 2, 2019.

[39] M. Luzuriaga, D. Berry, J. C. Reagan, R. A. Smaldone and J. J. Gassensmith, "Biodegradable 3D Printed Polymer Microneedles for Transdermal Drug Delivery," *Lab on a Chip,* vol. 18, no. 8, 2018.

[40] C. Yeung, S. Chen, B. King, H. Lin, K. King, F. Akhtar, G. Diaz, B. Wang, J. Zhu, W. Sun, A. Khademhosseini and S. Emaminejad, "A 3D-printed microfluidic-enabled hollow microneedle architecture for transdermal drug delivery," *Biomicrofluidics,* vol. 13, no. 6, 2019.

[41] M. R. Sarabi, S. A. Nakhjavani and S. Tasoglu, "3D-Printed Microneedles for Point-of-Care Biosensing Applications," *Micromachines,* vol. 13, no. 7, 2022.

[42] ScienceDaily, "Over 95% of the world's population has health problems, with over a third having more than five ailments," 08 June 2015. [Online]. Available: https://www.sciencedaily.com/releases/2015/06/150608081753.htm.

[43] J. A. Queenan, S. T. Wong, D. Barber, R. Morkem and A. Salman, "The Prevalence of Common Chronic Conditions Seen in Canadian Primary Care. Results from the Canadian Primary Care Sentinel Surveillance Network.," *Canadian Primary Care Sentinel Surveillance Network,* 2021.

[44] "Hospital stays in Canada, 2021–2022," Canadian Institute for Health Information, 2023. [Online]. Available: https://www.cihi.ca/en/hospital-stays-in-canada-2021-2022.

[45] T. Jasarevic, "WHO calls for worldwide use of "smart" syringes," World Health Organization, 23 February 2015. [Online]. Available: https://www.who.int/news/item/23-02-2015-who-calls-for-worldwide-use-of-smart-syringes#:~:text=There%20are%2016%20billion%20injections,blood%20transfusions%20and%20injectable%20contraceptives...

[46] ReportLinker, "Syringe Market Size & Share Analysis - Growth Trends & Forecasts (2023 - 2028)," Yahoo finance, 18 August 2023. [Online]. Available: https://finance.yahoo.com/news/syringe-market-size-share-analysis-165000816.html.

[47] R. Parhi and A. Mandru, "Enhancement of skin permeability with thermal ablation techniques: concept to commercial products," *Drug Delivery and Translational Research,* vol. 11, no. 3, p. 817–841, 2021.

[48] "Epidermis," Cleveland Clinic, 19 10 2021. [Online]. Available: https://my.clevelandclinic.org/health/body/21901-epidermis.

[49] T. Poonawalla and D. Diven, "Anatomy of the Skin," University of Texas Medical Branch, 2008. [Online]. Available: https://www.utmb.edu/pedi_ed/CoreV2/Dermatology/page_03.htm.

[50] "Hypodermis (Subcutaneous Tissue)," Cleveland Clinic, 19 10 2021. [Online]. Available: https://my.clevelandclinic.org/health/body/21902-hypodermis-subcutaneous-tissue.

[51] P.-C. Wang, B. A. Wester, S. Rajaraman, S.-J. Paik, S.-H. Kim and M. G. Allen, "Hollow Polymer Microneedle Array Fabricated by Photolithography Process Combined with Micromolding Technique," *Annual International Conference of the IEEE Engineering in Medicine and Biology Society,* p. 7026–7029, 2009.

[52] T. Liu, M. Chen, J. Fu, Y. Sun, C. Lu, G. Quan, X. Pan and C. Wu, "Recent advances in microneedles-mediated transdermal delivery of protein and peptide drugs," *Acta Pharmaceutica Sinica B,* vol. 11, no. 8, p. 2326–2343, 2021.

[53] "Microneedle drug delivery," Wikimedia Founation, Inc., 2024. [Online]. Available: https://en.wikipedia.org/wiki/Microneedle_drug_delivery#cite_note-9.

[54] H.-R. Jeong, H.-S. Lee, I.-J. Choi and J.-H. Park, "Considerations in the use of microneedles: pain, convenience, anxiety and safety," *Journal of Drug Targeting,* vol. 25, no. 1, pp. 29-40, 2017.

[55] A. Williams, Transdermal and Topical Drug Delivery from Theory to Clinical Practice, London: Pharmaceutical Press, 2003.

[56] N. Wilke, A. Mulcahy, S.-R. Ye and A. Morrissey, "Process optimization and characterization of silicon microneedles fabricated by wet etch technology," *Microelectronics Journal,* vol. 36, no. 7, pp. 650-656, 2005.

[57] H. P. Tham, K. Xu, W. Q. Lim, H. Chen, M. Zheng, T. G. S. Thng, S. S. Venkatraman, C. Xu and Y. Zhao, "Microneedle-Assisted Topical Delivery of Photodynamically Active Mesoporous Formulation for Combination Therapy of Deep-Seated Melanoma," *ACS Nano,* vol. 12, no. 12, pp. 11936-11948, 2018.

[58] G. Yan, K. S. Warner, J. Zhang, S. Sharma and B. K. Gale, "Evaluation needle length and density of microneedle arrays in the pretreatment of skin for transdermal drug delivery," *International Journal of Pharmaceutics,* vol. 391, no. 1-2, pp. 7-12, 2010.

[59] S. L. Banks, R. R. Pinninti, H. S. Gill, P. A. Crooks, M. R. Prausnitz and A. L. Stinchcomb, "Flux across microneedle-treated skin is increased by increasing charge of naltrexone and naltrexol in vitro," *Pharmaceutical Research,* vol. 25, p. 1677–1685, 2008.

[60] F. J. Verbaan, S. M. Bal, D. J. v. d. Berg, W. H. H. Groenink, H. Verpoorten, R. Lüttge and J. A. Bouwstra, "Assembled microneedle arrays enhance the transport of compounds varying over a large range of molecular weight across human dermatomed skin," *The Journal of Controlled Release,* vol. 117, no. 2, pp. 238-245, 2007.

[61] Y. Kapoor, M. Milewski, L. Dick, J. Zhang, J. R. Bothe, M. Gehrt, K. Manser, B. Nissley, I. Petrescu, P. Johnson, S. Burton, J. Moseman, V. Hua, T. Grunewald, M. Tomai and R. Smith, "Coated

microneedles for transdermal delivery of a potent pharmaceutical peptide," *Biomedical Microdevices,* vol. 22, no. 1, 2019.

[62] R. Haj-Ahmad, H. Khan, M. S. Arshad, M. Rasekh, A. Hussain, S. Walsh, X. Li, M.-W. Chang and Z. Ahmad, "Microneedle Coating Techniques for Transdermal Drug Delivery," *Pharmaceutics,* vol. 7, no. 4, p. 486–502, 2015.

[63] M. Cormier, B. Johnson, M. Ameri, K. Nyam, L. Libiran, D. D. Zhang and P. Daddona, "Transdermal delivery of desmopressin using a coated microneedle array patch system," *Journal of Controlled Release,* vol. 97, no. 3, pp. 503-511, 2004.

[64] M. R. Prausnitz, "Microneedles for transdermal drug delivery," *Advanced Drug Delivery Reviews,* vol. 56, no. 5, pp. 581-587, 2004.

[65] R. F. Donnelly, Microneedles for Drug and Vaccine Delivery and Patient Monitoring, John Wiley & Sons, Ltd, 2018.

[66] A. Sušić, Z. Hrnjica, I. Kajgana, M. Mujezinović, A. Hasanbegović, J. Brčkalo, A. Tucak, M. Sirbubalo and E. Vranić, "Use of Hollow Microneedle Drug Delivery Systems in Treatment of Diabetes Mellitus," in *CMBEBIH*, Bosnia and Herzegovina, 2019.

[67] S. R. Dabbagh, M. R. Sarabi, R. Rahbarghazi, E. Sokullu, A. K. Yetisen and S. Tasoglu, "3D-printed microneedles in biomedical applications," *iScience,* 2021.

[68] B. J. Park, H. J. Choi, S. J. Moon and H.-K. Han, "Pharmaceutical applications of 3D printing technology: current understanding and future perspectives," *Journal of Pharmaceutical Investigation,* vol. 49, no. 6, 2018.

[69] S. N. Economidou, D. A. Lamprou and D. Douroumis, "3D printing applications for transdermal drug delivery," *International Journal of Pharmaceutics,* vol. 544, no. 2, pp. 415-424, 2018.

[70] H. Bhuskute, P. Shende and B. Prabhakar, "3D Printed Personalized Medicine for Cancer: Applications for Betterment of Diagnosis, Prognosis and Treatment," *AAPS PharmSciTech,* vol. 23, no. 1, 2021.

[71] U. Roopavath and D. M. Kalaskar, 3D printing in medicine, Woodhead Publishing, 2017.

[72] V. Lancellota, S. Pagano, L. Tagliaferri and C. Aristei, "Individual 3-dimensional printed mold for treating hard palate carcinoma with brachytherapy: A clinical report," *Journal of Prosthetic Dentistry,* vol. 121, no. 4, 2018.

[73] M. M. Pillai, S. Ajesh and P. Tayalia, "Two-photon polymerization based reusable master template to fabricate polymer microneedles for drug delivery," *MethodsX,* vol. 10, 2023.

[74] C. W. Hull, "Apparatus for production of three-dimensional objects by stereolithography". United States Patent US4575330A, 8 8 1984.

[75] C. Schmidleithner and D. M. Kalaskar, "Stereolithography," in *3D Printing*, IntechOpen, 2018.

[76] Q. Mu, L. Wang, C. K. Dunn, X. Kuang, F. Duan, Z. Zhang, H. J. Qi and T. Wang, "Digital light processing 3D printing of conductive complex structures," *Additive Manufacturing,* vol. 18, p. 74–83, 2017.

[77] Q. Ge, A. H. Sakhaei, H. Lee, C. K. Dunn, N. X. Fang and M. L. Dunn, "Multimaterial 4D Printing with Tailorable Shape Memory Polymers," *Scientific Reports,* vol. 6, 2016.

[78] Y. Lu, G. Mapili, G. Suhali, S. Chen and K. Roy, "A digital micro-mirror device-based system for the microfabrication of complex, spatially patterned tissue engineering scaffolds," *J Biomed Mater Res A,* vol. 77, no. 2, pp. 396-405, 2006.

[79] E. Mathew, G. Pitzanti, E. Larrañeta and D. A. Lamprou, "3D Printing of Pharmaceuticals and Drug Delivery Devices," *Pharmaceutics,* vol. 12, no. 3, 2020.

[80] T. D. Ngo, A. Kashani, G. Imbalzano, K. T. Nguyen and D. Hui, "Additive manufacturing (3D printing): A review of materials, methods, applications and challenges," *Composites Part B: Engineering,* vol. 143, pp. 172-196, 2018.

[81] P. Soman, P. H. Chung, A. P. Zhang and S. Chen, "Digital microfabrication of user-defined 3D microstructures in cell-laden hydrogels," *Biotechnology and Bioengineering,* vol. 110, no. 11, pp. 3038-47, 2013.

[82] K. Rajan, M. Samykano, K. Kadirgama, W. S. W. Harun and M. M. Rahman, "Fused deposition modeling: process, materials, parameters, properties, and applications," *The International Journal of Advanced Manufacturing Technology,* vol. 120, p. 1531–1570, 2022.

[83] Y.-F. Chen, Y.-H. Wang and J.-c. Tsai, "Enhancement of surface reflectivity of fused deposition modeling parts by post-processing," *Optics Communications,* vol. 430, no. 10, 2018.

[84] A. S. Cordeiro, I. A. Tekko, M. H. Jomaa, L. Vora, E. McAlister, F. Volpe-Zanutto, M. Nethery, P. T. Baine, N. Mitchell, D. W. McNeill and R. F. Donnelly, "Two-Photon Polymerisation 3D Printing of Microneedle Array Templates with Versatile Designs: Application in the Development of Polymeric Drug Delivery Systems," *Pharmaceutical Research,* vol. 37, no. 174, 2020.

[85] R. Fitaihi, S. Abukhamees, S. H. Chung and D. Q. Craig, "Optimization of stereolithography 3D printing of microneedle micro-molds for ocular drug delivery," *International Journal of Pharmaceutics,* vol. 658, no. 2, 2024.

[86] S. N. Economidou, C. P. P. Pere, A. Reid, M. J. Uddin, J. F. C. Windmill, D. A. Lamprou and D. Douroumis, "3D printed microneedle patches using stereolithography (SLA) for intradermal insulin delivery," *Materials Science & Engineering C,* vol. 102, pp. 743-755, 2019.

[87] V. Yadav, P. K. Sharma, U. S. Murty, N. H. Mohan, R. Thomas, S. K. Dwivedy and S. Banerjee, "3D printed hollow microneedles array using stereolithography for efficient transdermal delivery of rifampicin," *International Journal of Pharmaceutics,* vol. 605, 2021.

[88] Y. Lu, S. N. Mantha, D. C. Crowder, S. Chinchilla, K. N. Shah, Y. H. Yun, R. B. Wicker and J.-W. Choi, "Microstereolithography and characterization of poly(propylene fumarate)-based drug-loaded microneedle arrays," *Biofabrication,* vol. 7, no. 4, 2015.

[89] I. Xenikakis, M. Tzimtzimis, K. Tsongas, D. Andreadis, E. Demiri, D. Tzetzis and D. G. Fatouros, "Fabrication and finite element analysis of stereolithographic 3D printed microneedles for transdermal delivery of model dyes across human skin in vitro," *European Journal of Pharmaceutical Sciences,* vol. 137, 2019.

[90] P. R. Miller, S. D. Gittard, T. L. Edwards, D. M. Lopez, X. Xiao, D. R. Wheeler, N. A. Monteiro-Riviere, S. M. Brozik, R. Polsky and R. J. Narayan, "Integrated carbon fiber electrodes within hollow polymer microneedles for transdermal electrochemical sensing," *Biomicrofluidics,* vol. 5, no. 1, 2011.

[91] S. V. Puttaswamy, G. V. Lubarsky, C. Kelsey, X. Zhang, D. Finlay, J. A. McLaughlin and N. Bhalla, "Nanophotonic-Carbohydrate Lab-on-a-Microneedle for Rapid Detection of Human Cystatin C in Finger-Prick Blood," *ACS Nano,* vol. 14, no. 9, 2020.

[92] J. G. Turner, E. Lay, U. Jungwirth, V. Varenko, H. S. Gill, P. Estrela and H. S. Leese, "3D-Printed Hollow Microneedle-Lateral Flow Devices for Rapid Blood-Free Detection of C-Reactive Protein and Procalcitonin," *Advanced Materials Technologies,* vol. 8, no. 16, 2023.

[93] M. Parrilla, A. Sena-Torralba, A. Steijlen, S. Morais, Á. Maquieira and K. D. Wael, "A 3D-printed hollow microneedle-based electrochemical sensing device for in situ plant health monitoring," *Biosensors and Bioelectronics,* vol. 251, 2024.

[94] W. Yao, D. Li, Y. Zhao, Z. Zhan, G. Jin, H. Liang and R. Yang, "3D Printed Multi-Functional Hydrogel Microneedles Based on High-Precision Digital Light Processing," *micromachines,* vol. 11, no. 1, 2020.

[95] Y. Liu, Q. Yu, X. Luo, L. Yang and Y. Cui, "Continuous monitoring of diabetes with an integrated microneedle biosensing device through 3D printing," *Microsystems & Nanoengineering,* vol. 7, no. 1, 2021.

[96] P. K. Monou, E. Andriotis, K. Tsongas, E. K. Tzimtzimis, O. L. Katsamenis, D. Tzetzis, P. A. Anastasiadou, C. Ritzoulis, I. Vizirianakis, D. Andreadis and D. G. Fatouros, "Fabrication of 3D Printed Hollow Microneedles by Digital Light Processing for the Buccal Delivery of Actives," *ACS Biomaterials Science & Engineering,* vol. 9, no. 8, 2023.

[97] X. Wang, M. Jiang, Z. Zhou, J. Gou and D. Hui, "3D printing of polymer matrix composites: A review and prospective," *Composites Part B: Engineering,* vol. 110, pp. 442-458, 2017.

[98] A. Khosraviboroujeni, S. Z. Mirdamadian, M. Minaiyan and A. Taheri, "Preparation and characterization of 3D printed PLA microneedle arrays for prolonged transdermal drug delivery of estradiol valerate," *Drug Delivery and Translational Research,* vol. 12, no. 5, p. 1195–1208, 2021.

[99] M. Camović, A. Biščević, I. Brčić, K. Borčak, S. Bušatlić, N. Ćenanović, A. Dedović, A. Mulalić, M. Osmanlić, M. Sirbubalo, A. Tucak and E. Vranić, "Coated 3D Printed PLA Microneedles as Transdermal Drug Delivery Systems," in *IFMBE Proceedings, Vol. 73*, Springer, 2019.

[100] Z. F. Rad, P. D. Prewett and G. J. Davies, "High-resolution two-photon polymerization: the most versatile technique for the fabrication of microneedle arrays," *Microsystems & Nanoengineering,* vol. 7, no. 71, 2021.

[101] A. Ovsianikov, B. Chichkov, P. Mente, N. A. Monteiro-Riviere, A. Doraiswamy and J. Narayan, "Two Photon Polymerization of Polymer–Ceramic Hybrid Materials for Transdermal Drug Delivery," *International Journal of Applied Ceramic Technology,* vol. 4, no. 1, pp. 22-29, 2007.

[102] B. Szeto, A. Aksit, C. Valenti, M. Yu, E. G. Werth, S. Goeta, C. Tang, L. M. Brown, E. S. Olson, J. W. Kyasar and A. K. Lalwani, "Novel 3D-printed hollow microneedles facilitate safe, reliable, and informative sampling of perilymph from guinea pigs," *Hearing Research,* 2021.

[103] A. Aksit, S. Rastogi, M. L. Nadal, A. M. Parker, A. K. Lalwani, A. C. West and J. W. Kysar, "Drug delivery device for the inner ear: ultra-sharp fully metallic microneedles," *Drug Delivery and Translational Research,* vol. 11, no. 1, p. 214–226, 2021.

[104] P. R. Miller, X. Xiao, I. Brener, D. B. Burckel, J. Narayan and R. Polsky, "Microneedle-Based Transdermal Sensor for On-Chip Potentiometric Determination of K,(+)," *Advanced Healthcare Materials,* vol. 3, no. 6, 2014.

[105] M. Razzaghi and M. Akbari, "The Effect of 3D Printing Tilt Angle on the Penetration of 3D-Printed Microneedle Arrays," *micromachines,* vol. 14, no. 6, 2023.

[106] M. R. Sarabi, A. Ahmadpour, A. K. Yetisen and S. Tasoglu, "Finger-Actuated Microneedle Array for Sampling Body Fluids," *Applied Sciences,* vol. 11, no. 12, 2021.

[107] Q. K. Anjani, A. D. C. Nainggolan, H. Li, A. Miatmokol, E. Larrañeta and R. F. Donnelly, "Parafilm® M and Strat-M® as skin simulants in in vitro permeation of dissolving microarray patches loaded with proteins," *International Journal of Pharmaceutics,* vol. 655, 2024.

[108] E. Larrañeta, J. Moore, E. M. Vicente-Pérez, P. González-Vázquez, R. Lutton, A. D. Woolfson and R. F. Donnelly, "A proposed model membrane and test method for microneedle insertion studies," *International Journal of Pharmaceutics,* vol. 472, no. 1-2, pp. 65-73, 2014.

[109] A. Khorshidian, N. Sharifi, F. C. Kheirabadi, F. Rezaei, S. A. Sheikholeslami, A. Ariyannejad, J. Esmaeili, H. Basati and A. Barati, "In Vitro Release of Glycyrrhiza Glabra Extract by a Gel-Based Microneedle Patch for Psoriasis Treatment," *Gels,* vol. 10, no. 2, 2024.

APPENDIX

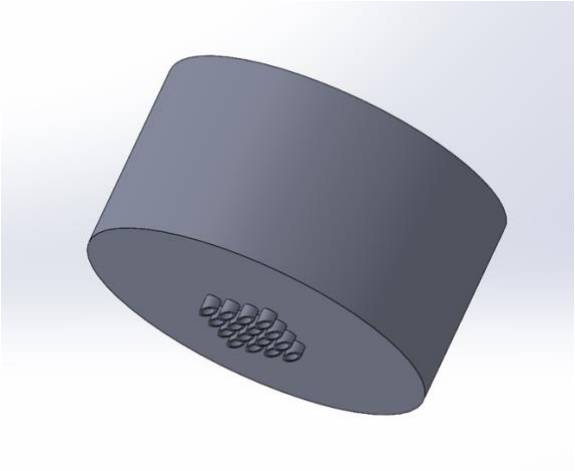

Figure 11: Isometric view of the CAD model of the drug delivery chamber. Notice the 4x4 MN array at the bottom.

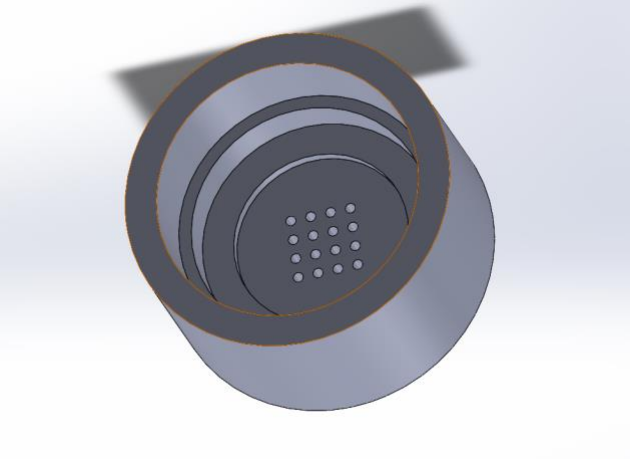

Figure 12: Inside view of the CAD model of the drug delivery MN chamber. Notice the steps for the ultrasonic membrane to sit tightly above the top of the lumens of the MNA.

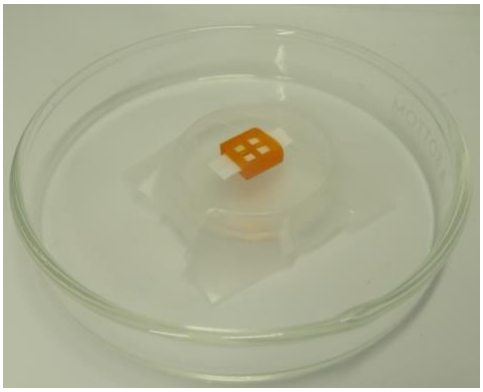

Figure 13: The setup shows sensing MNA placed on the membrane on the biomarker loaded DI water. Notice that four test strips are placed, with 3 being blank strips and one being a coated pH test strip.

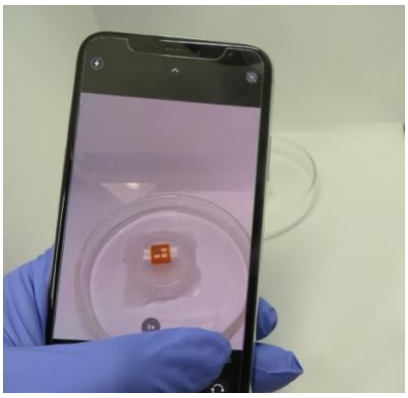

Figure 14: Taking a photo of the detection strips using a smartphone.

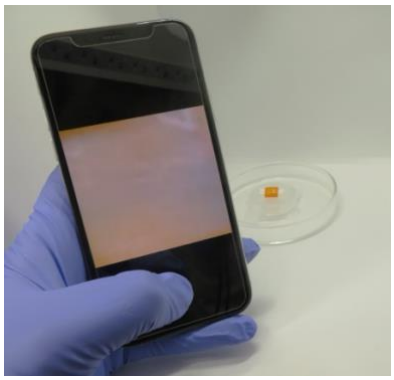

Figure 15: Visualizing a zoomed-in view for viewer's reference.

Figure 16: The applications UI displays average RGB values (from 0-255), image of the average color, average RGB percentage values and detected biomarker values.

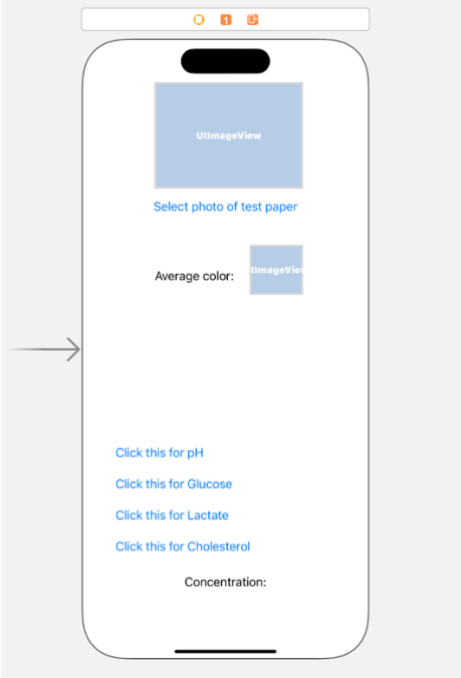

Figure 17: A closer look at biomarker detection UI in Xcode UI editor. Numerical values of RGB, the image of average color and its RGB values, as well as the concentration are not displayed until the test paper photo is selected.

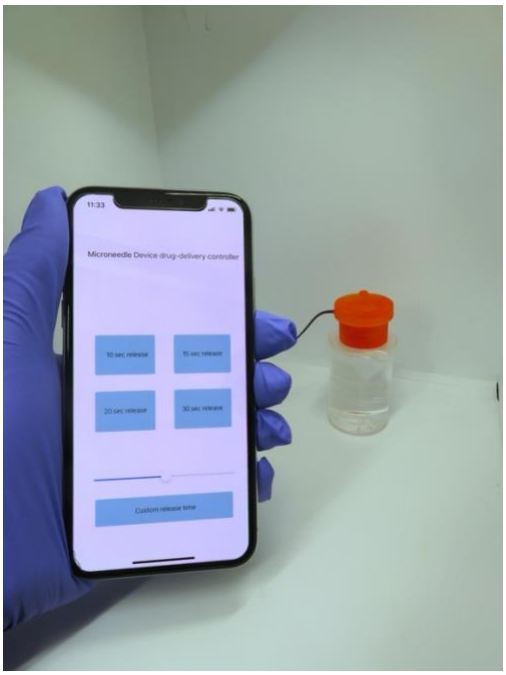

Figure 18: This figure shows a UI for drug-delivery application. Notice the drug delivery MNA with the reservoir placed on the beaker with membrane seal.

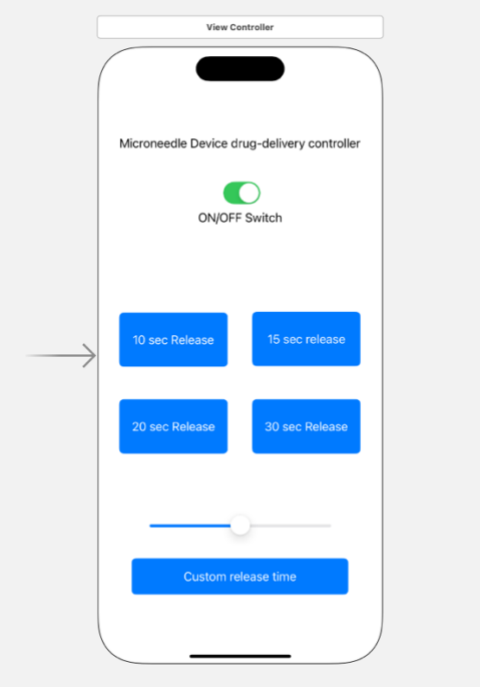

Figure 19: A closer look at the UI for drug delivery control in Xcode UI editor.

Time (min)	Amount Penetrated (mg/cm2)	
0	0.00000123	0.00000123
2	0.000256	0.000252
4	0.00057	0.000564
10	0.000684	0.000551
20	0.000582	0.000699
30	0.00055	0.000706
32	0.00121	0.001343
34	0.001194	0.001213
40	0.001237	0.001244
50	0.001196	0.001191
60	0.001229	0.001215
62	0.001904	0.00193
64	0.001955	0.00192
70	0.001921	0.00187
80	0.001829	0.001866
90	0.001894	0.001911
92	0.002451	0.002584
94	0.002534	0.002527
100	0.00253	0.002522
110	0.002556	0.002593
120	0.002583	0.002622

Table 2: Concentration of Rhodamine B detected in ON/OFF drug delivery test using fluorescence spectroscopy.

pH	Red		Green		Blue	
3	55.74468	49.29577	41.2766	42.25352	2.978723	8.450704
4	49.15254	46.47059	41.24294	41.17647	9.60452	12.35294
5	43.81443	44.21365	42.26804	40.35608	13.91753	15.43027
6	43.07692	45.77778	40.61538	39.55556	16.30769	14.66667
7	41.88034	37.28814	39.88604	39.83051	18.23362	22.88136
8	27.73723	19.67213	33.57664	32.37705	38.68613	47.95082

Table 3: RGB values as a fraction of the summation of RGB values for pH detection.

Glucose Concentration (mM)	Red			Green			Blue		
0	62.28074	60.59747	49.48794	63.36675	59.33065	49.64402	61.89773	59.72042	51.01119
2	65.09077	67.22392	65.54871	61.53389	58.82093	59.37135	44.46091	44.956	46.67343
4	64.95576	70.03848	67.90192	62.4209	57.76897	58.58966	43.40946	41.92084	44.23325
6	68.19755	71.19673		58.79099	56.86783		43.50533	41.19559	
8	66.8983	74.53867	69.7711	61.72165	55.77723	59.5521	41.41323	36.50873	39.81886
10	66.0981	75.09887	72.47271	60.82431	54.85946	56.41119	43.9482	36.75051	39.56618
12	66.58406	76.71584	72.52445	61.03539	54.50862	56.48889	42.90973	33.81553	39.36
14	70.95502	77.60498	73.33503	57.74531	53.58439	56.07973	40.38397	33.25928	38.43226
16	71.00106	76.65054	73.55999	59.32965	53.60178	58.36826	37.93207	35.37717	34.3813

Table 4: RGB values as a fraction of the summation of RGB values for Glucose detection.

Lactate Concentration (mM)	Red				Green				Blue			
0	35.688	35.815	35.988	36.283	34.783	33.4	35.398	34.808	29.529	30.785	28.614	28.909
0.4	35.37	35.897	36.275	35.89	34.63	34.266	35.621	34.969	30	29.837	28.105	29.141
0.8	35.922	36.49	36.304	36.076	35.146	34.873	35.974	36.392	28.932	28.637	27.723	27.532
1.2	36.05	36.16	35.9	37.78	35.19	34.46	35.9	37.78	28.76	29.38	28.21	24.44
1.6	35.38	36.07	36.68	36.82	35.17	34.9	36.68	36.43	29.45	29.03	26.64	26.74
2	35.52	36.34	36.6	36.28	35.29	35.09	36.6	36.28	29.19	28.57	26.79	27.43
2.4	35.71	36.2	36.86	35.71	35.06	34.66	36.86	36.11	29.22	29.14	26.27	28.17
2.8	36.08	35.86	36.3	35.62	35.61	34.69	36.65	35.62	28.3	29.45	27.05	28.76
3.2	37	37.78	37.8	36.76	36.25	36.51	37.8	37.13	26.75	25.71	24.41	26.1

Table 5: RGB values as a fraction of the summation of RGB values for Lactate detection.

Note that in the mobile application for biomarker detection, RGB values were represented as a fraction with respect to the mean RGB value of the image and not as a fraction of the summation of RGB values for each image. Those values were used in MATLAB to find the calibration curves. It must be noted that both normalization methods yield the same results for the scope of this project.